

Groot onderzoek: Chemical evolution of the
Sculptor dwarf spheroidal galaxy and its
implications on the Epoch of Reionization

Maarten A. Breddels
supervisors: Eline Tolstoy & Saleem Zaroubi

February 11, 2009

Abstract

We develop a galactic chemical evolution for Sculptor which is able to reproduce the metallicity distribution functions (MDFs) of Mg, Ca and Fe. The relative star formation history from the literature is converted to an absolute star formation history by calculating the average star formation rate from CMD analysis. Because of the spatial sampling and the metallicity gradient present in Sculptor we have to correct its observed MDFs. The star formation history and the corrected MDF combined with a galactic chemical evolution model allows us to derive the inflow rate of primordial gas onto Sculptor and the amount of metals ejected into the intergalactic medium. The rate of inflow is constrained by the corrected Ca MDF.

Since dwarf galaxies were probably dominant during the end of the Universe's Dark Ages, we use Sculptor as a template to study their influence on the ionization of the intergalactic medium. We assume these dwarf galaxies are populated by PopII stars. Using the STARBUST99 software packet, we calculate the production rate of ionising photons based on the star formation rate of Sculptor. Using the Press-Schechter formalism and a scaling relation for the star formation rate relative to that of Sculptor we create a model for the reionization history of the Universe. We find that ancient stellar populations in dwarf galaxies such as Sculptor are sufficient to ionize the Universe at the assumed epoch of reionization of $z = 6.5$.

Contents

| | | |
|----------|--------------------------------------|-----------|
| 1 | Introduction | 4 |
| 2 | Background | 8 |
| 2.1 | Chemical evolution | 8 |
| 2.1.1 | The Simple model | 8 |
| 2.1.2 | Outflow | 11 |
| 2.1.2.1 | Leaky box model | 12 |
| 2.1.2.2 | Metal ejection | 13 |
| 2.1.3 | Inflow | 13 |
| 2.2 | Sources of metals | 14 |
| 2.2.1 | Intermediate mass yields | 16 |
| 2.2.2 | Type II supernova yields | 16 |
| 2.2.3 | Type Ia supernova yields | 16 |
| 2.3 | Press Schechter | 16 |
| 3 | Sculptor | 21 |
| 3.1 | Data | 22 |
| 3.1.1 | Photometry | 22 |
| 3.1.2 | Metallicities | 26 |
| 3.2 | The star formation history | 29 |
| 3.3 | Total metallicity | 31 |
| 3.4 | GCE model | 31 |
| 3.5 | Results | 34 |
| 3.6 | Discussion | 37 |
| 4 | Reionization | 39 |
| 4.1 | Model | 41 |
| 4.1.1 | Star formation rate | 41 |
| 4.1.2 | Halo mass function | 41 |
| 4.1.3 | Ionizing photons | 41 |
| 4.1.4 | Recombination | 42 |

| | | |
|----------|----------------------------------|-----------|
| 4.1.5 | Mean free path | 44 |
| 4.1.6 | Thompson optical depth | 44 |
| 4.2 | Results | 45 |
| 4.2.1 | Ionizing photons | 45 |
| 4.2.2 | Recombination | 47 |
| 4.2.3 | Reionization model | 48 |
| 4.3 | Discussion | 51 |
| 5 | Summary | 52 |

Chapter 1

Introduction

Most inflationary models predict a primordial power spectrum of the form $P(k) \propto k$, where k is the wavenumber. Depending on the true nature of the dark matter (DM), the structure in the Universe forms top-down or bottom-up (hierarchical). According to the most popular cosmological model, the so called Λ -cold dark matter (CDM) model, small structures have formed first, i.e. hierarchical structure formation. In this model, the larger galaxies (such as the Milky Way) were formed out of many smaller galaxies, while these building blocks themselves may again be built by yet smaller galaxies. In the Λ CDM model, small galaxies are therefore considered to be the building blocks of many of the larger galaxies we see today. Note that in this scenario, large galaxies at early times are not absent they are just rare.

In this cosmological scenario, our Milky Way has accreted many small galaxies in the past, and we can still see this merging happening today, e.g. the Sagittarius stream (Ibata et al., 1994; Majewski et al., 2003). The hierarchical build-up of our galaxy complicates the study of its formation history as it consists of a mixture of stars formed in situ, and stars which have been accreted at different times from smaller galaxies. Past merging events can be identified in, for instance, the phase space distribution of stars in the Milky Way (Helmi et al., 2006b). Is it also possible to study the building blocks of our Milky Way by looking at its dwarf satellites? Are these galaxies equivalent to the building blocks accreted by our Galaxy at higher redshift? Did they evolve in the same way as these building blocks, but have not yet merged with a larger system? I will not attempt to answer these questions, but one should be aware that the answers are not straight forward. For instance the abundance patterns of individual stars from dwarfs are often different from that of the Milky Way halo (e.g. Shetrone et al., 2001; Tolstoy et al., 2003; Venn et al., 2004). For example, the very low $[\text{Fe}/\text{H}]$ (< -3.5) stars which are found in our Milky Way halo, have not been found in dwarf galaxies. Thus it seems likely that if these low metallicity stars are present in dwarf galax-

ies, their fraction is significantly lower than in the Milky Way halo (Helmi et al., 2006a). Thus, abundance patterns seen in individual stars in present day dwarfs are not seen in our Milky Way. This result seems inconsistent with the merger scenario. However, if our hierarchical merger scenario is correct the difference in abundance patterns imply that the present day dwarfs are unlike the building blocks of the Milky Way. Although these dwarf galaxies possible are not exactly like the building blocks of our Galaxy, they are the closest match to the small galaxies that formed in the early Universe.

Dwarf galaxies are one of the oldest and simplest structures in the Local Group, making them interesting probes of star formation in the high redshift Universe. Local Group dwarf galaxies, such as the Sculptor dwarf spheroidal (dSph), are close enough to allow us to observe individual stars. This enables us to create colour magnitude diagrams (CMDs) of the stellar populations in these galaxies. By comparing the observed CMD to stellar models (isochrones) we can infer the star formation history (SFH) of the galaxy (see e.g. Skillman et al. (2003)).

The proximity of Local Group galaxies also makes it possible to take spectra of individual bright red giant branch (RGB) stars. From these spectra one can determine the abundances of numerous individual elements depending on the resolution and the wavelength range of the spectrum. The metal¹ content of the stellar photospheres gives us detailed information on the composition of the interstellar medium (ISM) out of which the star formed. This does assume that the photosphere remain 'pristine', meaning that none of the new metals that form in the core of the star reach the surface, no original metals in the photosphere 'sink' into the core and no metals are accreted from the ISM. Assuming that the atmospheres of stars trace the metal composition of the ISM at the date of birth, then they make outstanding tracers of the chemical evolution of the galaxies that host them. Notice however, that these assumptions are not always valid. For example, some metals like C, N and O can reach the upper layers of a star during a so called dredge-up phase. During this phase, the outer envelope of a star and its deeper layers are mixed due to convection. For heavier metals (Ca, Ti, Fe, ...) in the atmospheres of old (> 1 Gyr old) RGB stars this is not an issue, since these low mass ($\sim 0.8M_{\odot}$) stars do not form these metals.

There are good reasons to focus on Local Group dwarf galaxies. If they are similar to the galaxies that merged in the past with our Galaxy, we can the study individual ingredients of our Milky Way separately. The small size of the dwarf galaxies also makes them convenient to study: they are less complex. Instead of being the composite of multiple small galaxies like our Milky Way, the dwarfs will have experienced none or very few mergers. Also the small total number of stars compared to the Milky Way ($\sim 10^{11}$ in the Milky Way versus $\sim 10^6$ for

¹In astronomy metal refers to all elements heavier than Helium.

small dwarfs like Sculptor) gives a computational benefit to simulations. In principle this makes dwarf galaxies easier to simulate and analyse, but their distance makes acquiring stellar data more time consuming than for instance data from our Galaxy. There are exceptions such as the Small Magellanic Cloud (SMC) and the Sagittarius stream, which are very nearby, however, their tidal disruption by the Milky Way make them complex to interpret in terms of formation and evolution.

Since dwarf galaxies are one of the simplest galaxies, they make studying their chemical evolution less complex than e.g. the Milky Way. Galactic chemical evolution (GCE) models began with the work of Tinsley (1979). These models use theoretical yields of supernovae (SNe), analytical laws for star formation, outflow, inflow etc, and thus make predictions about the abundance patterns and the distribution of metallicities and ages for the stellar population in a galaxy (e.g. Lanfranchi and Matteucci, 2003; Marcolini et al., 2006). Instruments like VLT/FLAMES allow spectra to be taken for large samples of stars from dwarf galaxies, which gives us abundances for numerous elements for ~ 100 stars per galaxy per observation (Hill et al., in preparation, Letarte, 2007 PhD). These data allow us to put useful constraints on the GCE of dwarf galaxies.

In this work we will also investigate the role dwarf galaxies may have in the reionization of the Universe. Since the Λ CMD scenario predicts large numbers of low mass galaxies throughout the Universe, at low and high redshifts, dwarf galaxies may have been important during the epoch of reionization (EoR). Between the surface of last scattering (at $z \approx 1100$) and now, the Universe became reionized. From the imprint of the neutral hydrogen on the spectra of quasars (QSOs), the so-called Gunn-Peterson effect (Gunn and Peterson, 1965), we know that the Universe became highly ionized at $z \lesssim 6.5$. The earliest star formation is predicted to occur around $z \approx 15 - 20$, which leaves $\sim 0.6 - 0.7$ Gyr between these two epochs in which the Universe became ionized.

Here we will use the Sculptor dSph galaxy as a template for a galaxy that formed in the early Universe ($z > 6$). To date no accurate and precise SFH has been determined for Sculptor. We have data available which does not go as deep as the older main sequence turn-off (MSTO), however from CMD analysis and the presence of a blue and red horizontal branch, we do know that Sculptor formed most of its stars at high redshifts (e.g. Mateo, 1998; Tolstoy et al., 2001). Therefore we take the SFH of Sculptor as a single value at high redshift. New observations of Sculptor (de Boer et.al., in preparation) will provide a more details SFH in the near future. From the available high resolution (HR) abundance determination for ~ 90 stars in Sculptor, combined with the ~ 470 low resolution (LR) calcium triplet (CaT) measurements we construct a semi-empirical GCE model. Our model is able to predict the (net) inflow of gas and the amount of metals that are not confined to the star forming regions. The star formation rate of Sculptor is assumed to be constant and assumed to be representative of the average star

formation rate of galaxies of $10^8 M_{\odot}$ at high redshifts. We use the Press Schechter formalism (Press and Schechter, 1974; Sheth and Tormen, 2002) to determine the number of galaxies for different masses at each redshift. Combining this with the star formation rate allows us to create a reionization model using only PopII stars as ionization sources.

This report is structured as follows: In §2 we explain background material which is needed to understand the rest of the report. Then in §3 we develop a model for Sculptor, making an estimate of the star formation rate (SFR), and its chemical history. Using the Press-Schechter formalism and the results from §3, we develop a reionization model of the Universe in §4. We end with a summary in §5.

Chapter 2

Background

2.1 Chemical evolution

It was Sir Frey Hoyle (Hoyle, 1946, 1954) who first realised that stars are responsible for the production of (heavy) metals. This led to the publication of classical paper of Burbidge et al. (1957), referred to as B²FH. This theory of stellar nucleosynthesis then led to the study of the evolution of the metal abundances in galaxies, now referred to as galactic chemical evolution (GCE). The Simple one-zone model (Schmidt, 1963) is the default framework in which GCE is placed. Despite being an unrealistic model, and not corresponding very well to measurements, it is still a good starting point for understanding GCE. Current models of supernova (SN) explosions and their yields allow us to explore complicated models in which the evolution of many elements can be traced.

First we want to start from simple models for which analytic solutions exist or that are easy to understand. From these simple models we can develop a better feeling for certain quantities, such as the yields, and what they represent and how they are reflected in measured data. A more complicated model, such as for Sculptor (§3), can then be understood in terms of the more simple model.

2.1.1 The Simple model

The so called *Simple Model* is often used as a point of comparison with other models. It is based on the following assumptions:

1. The system is closed, no gas flows in or out of the system (*closed box model*).
2. There are two kinds of stars, the lower mass star which live forever, and the high mass stars which die instantaneously and add their elements to

the interstellar medium (ISM) by SN explosions (*Instantaneous Recycling Approximation (IRA)*).

3. The gas is always well mixed, meaning that all new metals are directly available for the next generation of stars (*Instantaneous Mixing Approximation (IMA)*).
4. The initial mass function (IMF) is constant in time.

The closed box assumptions can be translated into the following equations:

$$\begin{aligned} M_*(t) + M_g(t) &= M = \text{const}, \\ dM_*(t) &= -dM_g(t), \end{aligned} \quad (2.1)$$

where $M_*(t)$ is the mass in stars (and remnants), $M_g(t)$ is the mass in gas in the system (composed of hydrogen, helium and all the metals) and M the total mass of the system, which is constant.

The IMF determines the distribution of the masses of the stars. For simplicity a single power law in the form of a Salpeter IMF is used:

$$\phi(m) \propto m^{-2.35}, \quad (2.2)$$

where m is the initial mass of the star. We normalise the IMF such that it can be interpreted as a probability distribution function (pdf):

$$\int_{m_l}^{m_h} \phi(m) dm = 1, \quad (2.3)$$

where m_l and m_h are the low and high mass cut-offs of the distribution, typical values range from $m_l = 0.08 - 0.1$ and $m_h = 40 - 200$. If R is the return fraction (in mass) of a stellar generation then $\alpha = 1 - R$ is the lockup fraction, the fraction of mass which remains in stars and remnants.

Using the star formation rate ψ , we can write the following differential equations:

$$\begin{aligned} \frac{dM_g}{dt} &= -\alpha\psi, \\ \frac{dM_*}{dt} &= \alpha\psi, \\ \frac{dM_{i,g}}{dt} &= \frac{d(Z_{g,i}M_g)}{dt} \\ &= P_i\psi - Z_{i,g}\alpha\psi = y_i\alpha\psi - Z_{i,g}\alpha\psi \\ &= (y_i - Z_{i,g})\frac{dM_*}{dt} \end{aligned} \quad (2.4)$$

where $Z_{g,i} = M_{g,i}/M_g$ is the mass abundance of the gas for element i , P_i is the amount of metals produced per unit mass converted to stars, and y_i is called the yield. In the case of a closed box model, the yield y_i can be related to P_i ($y_i = \alpha^{-1}P_i$), and is also called the true yield ($y_{i,\text{true}}$) because it is related to sum of metals produced by stars. In non-closed box models, while the true yield stays the same, processes like outflow can decrease the metals available for subsequent generations of stars. The yield is then referred to as the effective yield ($y_{i,\text{eff}}$). Although the physical meaning of the yield (y_i or $y_{i,\text{eff}}$) may not be obvious (since it's expressed as a ratio of metals produced per mass locked up), this important quantity is convenient for the analytical solutions, as we will see in the next sections.

To solve the differential equations above using 2.1, we write:

$$\begin{aligned} \frac{d(Z_{g,i}M_g)}{dt} &= \frac{dZ_{g,i}}{dt}M_g + Z_{g,i}\frac{dM_g}{dt}, \\ \frac{dZ_{g,i}}{dt} &= \frac{1}{M_g} \left((y_i - Z_{i,g})\frac{dM_*}{dt} + Z_{g,i}\frac{dM_*}{dt} \right), \\ &= \frac{y_i}{M_g} \frac{dM_*}{dt} = -\frac{y_i}{M_g} \frac{dM_g}{dt}. \end{aligned} \quad (2.5)$$

This equation easily be solved for $Z_{g,i}(t)$, resulting in:

$$Z_{i,g}(t) = y_i \ln \left(\frac{M_g(t=0)}{M_g(t)} \right) = y_i \ln \left(\frac{M}{M_g(t)} \right) + Z_{i,g}(0), \quad (2.6)$$

which is often written using the gas fraction $\mu = M_g/M$:

$$Z_{i,g}(t) = y_i \ln(\mu^{-1}) + Z_{i,g}(0), \quad (2.7)$$

We can rewrite this as the cumulative stellar mass below a certain abundance Z' :

$$M_*(Z < Z') = M \left(1 - e^{-\frac{Z_{i,g}(t)-Z_{i,g}(0)}{y_i}} \right). \quad (2.8)$$

When we differentiate this to Z , we find the distribution of mass as function of metallicity:

$$\begin{aligned} \frac{dM_*}{dZ} &= M \frac{1}{y_i} e^{-\frac{Z_{i,g}(t)-Z_{i,g}(0)}{y_i}}, \\ \frac{dM_*}{d \log Z} &= \ln(10) M \frac{Z_{i,g}}{y_i} e^{-\frac{Z_{i,g}(t)-Z_{i,g}(0)}{y_i}}. \end{aligned} \quad (2.9)$$

where $Z_{i,g}(0) = 0$ is often assumed¹.

¹In Eq. 2 of Prantzos (2008) the substitution $d \log Z' = Z/(Z - Z_0) d \log Z$ might be missing, giving a very different result.

The stellar mass M_* can be translated into a number of stars (by dividing it by the mean mass of surviving stars). We can now see Eq. 2.9 as being proportional to the number of stars in a given bin of $\log Z$. This makes it possible to compare histograms of observed stellar abundances to this model. We also note that the star formation rate (SFR) does not enter the solution. This means that the time evolution of the galaxy has no influence on the metallicity distribution of its stars (for this Simple model). Note that this is only valid under the assumptions of the Simple model (most importantly the IRA). The distribution of stars as a function of metallicity is often referred to as the metallicity distribution function (MDF).

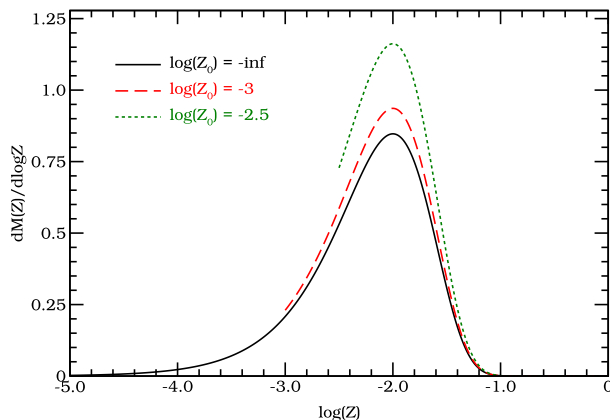


Figure 2.1: MDF for the Simple model, as determined by Eq. 2.9. The shape of the function is independent of the SFH and yield. Changing the yield can only move the curve left or right.

In Fig. 2.1 we plot the MDF, assuming the Simple model, for a yield of $y_i = 0.01$ and for different values of $Z_{g,i}(0)$. For models with $Z_{g,i}(0) > 0$ and an equal amount of stars formed, no low metallicity stars exist, thus increasing the number of high metallicity stars. The characteristic shape of the distribution however, does not change, it merely misses the low metallicity tail. The figure shows the MDF peaks at $Z_{g,i} = y_i = 0.01$, which can also be derived from Eq. 2.9. A different yield, SFHs or initial gas mass will not change the shape of MDF, only the total amount of stars produced and the location of the peak. A MDF that differs from Fig. 2.1 must therefore be due to violations of the assumptions of the Simple Model. Note that all gas is converted into stars in these models.

2.1.2 Outflow

A natural extension to the closed box model, it to let mass flow out of the system. Here we discuss two extremes of outflow. The leaky box model lets gas escape

into the intergalactic medium (IGM) which is of the same chemical composition of the ISM at the time of ejection. The second model assumes only metals escape the galaxy.

2.1.2.1 Leaky box model

This model can be interpreted as outflow caused by stellar feedback. The energy output of the stars can heat the gas, giving it enough energy to escape the host galaxy. It is therefore natural to assume the outflow of gas to be proportional to the SFR. In this case, we assume the composition of the outflow is similar to the composition to the gas (homogeneous outflow), and the proportionality constant is taken to be η .

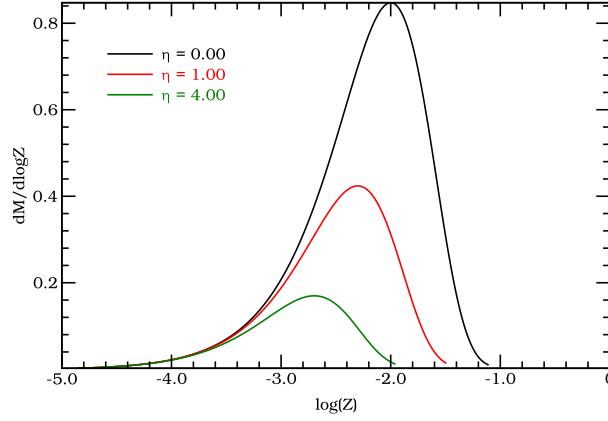


Figure 2.2: Distribution of stellar mass as function of metallicity per log bin for the Leaky box model. The shape of the function is similar to that of the Simple model.

If we modify Eqs. 2.4 to include the outflow, we get:

$$\begin{aligned} \frac{dM_g}{dt} &= -\alpha\psi - \alpha\psi\eta, \\ \frac{dM_*}{dt} &= \alpha\psi, \\ \frac{dM_{i,g}}{dt} &= (y_i - Z_{i,g})\frac{dM_*}{dt} - Z_{i,g}\alpha\psi\eta, \end{aligned} \quad (2.10)$$

for which we can find an analytical solution to the MDF:

$$\frac{dM_*}{d \ln Z} = M \frac{Z_{i,g}}{y_i} e^{-\left(\frac{Z_{i,g}(t) - Z_{i,g}(0)}{y_i}\right)(1+\eta)}, \quad (2.11)$$

where $\eta > 0$ is used to describe the amount outflow relative to the SFR. The resulting MDFs are shown in Fig. 2.2 for different values of η . The substitutions $y_i = y'_i/(1 + \eta)$ and $M = M'/(1 + \eta)$ in Eq. 2.9 will reproduce the same result as Eq. 2.11, which analytically shows that the characteristic shape of the MDF will not be changed by homogeneous outflow. Note that this outflow changes the effective yield $y_{i,\text{eff}} = y_{i,\text{true}}/(1 + \eta)$ and lowers the available mass for stars by a factor $(1 + \eta)$ as reflected by the area under the curves in Fig. 2.2.

2.1.2.2 Metal ejection

If a part of the metals ejected by SN escape the galaxy (or at least the star forming region), the effective yields simply get reduced by $y_{i,\text{eff}} = (1 - f_{\text{esc},Z})y_{i,\text{true}}$, with $f_{\text{esc},Z}$ the escape fraction of metals. Note also that this only changes the yield, which does not change the shape of the MDF.

2.1.3 Inflow

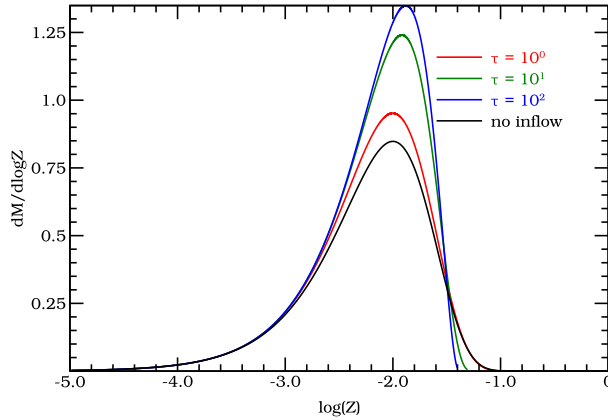


Figure 2.3: MDF for the inflow model (red, green and blue) and the Simple model (black). Note that the inflow models have a different shape compared to the Simple model.

The accretion of gas onto galaxies is a likely process to occur in galaxy formation, and is also seen in nearby galaxies and our own. We assume that the metallicity of the in-falling gas is always lower than the current metallicity of the ISM, such that the amount of metals accreted can be neglected. If we modify Eqs.

2.4 to include the inflow, we get:

$$\begin{aligned}\frac{dM_g}{dt} &= -\alpha\psi + \dot{M}_{\text{inflow}}, \\ \frac{dM_*}{dt} &= \alpha\psi, \\ \frac{dM_{i,g}}{dt} &= (y_i - Z_{i,g})\frac{dM_*}{dt},\end{aligned}\tag{2.12}$$

where the most common assumption for $\dot{M}_{\text{inflow}}(t) = \dot{M}_{\text{inflow}}(0)e^{-t/\tau}$ (Chiosi, 1980), where τ is a characteristic timescale. In this case, there is no analytical solution independent on time (and therefore the SFH) for the MDF. Therefore we solve the solutions numerically, with the results shown in Fig. 2.3 for different values of τ , where we have assumed a constant SFR. The absolute values of τ are not important, but the model demonstrates that this inflow model can alter the characteristic shape of the MDF.

Since we assumed the SFR is constant, the production rate of metals is also constant in time. This means that the time period between $\log(Z_i) = -5$ to -3 is very short compared to e.g. $\log(Z_i) = -3$ to -1 . This means that the low metallicity tail is formed in a very short time span, and therefore is not that much affected by the inflow of metal free gas (even though the inflow rate is highest at $t = 0$). After the ISM reaches a higher metallicity the inflow becomes important, and helps keeping the metallicity of the ISM stay low. This causes more intermediate metallicity stars to be created relative to the Simple model.

2.2 Sources of metals

In the previous section we discussed GCE models, which all depend on the yield y_i . If all galaxies behaved like the Simple model, then for a given element, the MDFs for all galaxies of all masses should be equal. In this case the yield can simple be measured from the MDF. However, reality is more complex, since not all MDFs are similar, as the mass-metallicity relations demonstrates (Lequeux et al., 1979). A different approach is to make models for stars and supernova explosions (SNe), and get the yields from these.

The sources of metals in the Universe are the stars, supernovae in particular. All stars form helium and metals by fusion in their core or shells. The low and intermediate stars ($M \lesssim 8M_\odot$) can dredge up these metals from their core into their photosphere. By means of stellar winds, or the planetary nebulae (PN) phase, they can lose their outer shells with metals and thereby enrich the ISM. Depending on their initial mass, stars produce different amounts of heavy elements leading to a variety of abundance patterns in their expelled material.

The heavier stars ($M \gtrsim 8M_{\odot}$) end their lives with a core of iron unable to sustain hydrostatic equilibrium. This leads to a core collapse phase, where the outer shells bounce back from the core. A large fraction of the envelope, rich in α elements², gets expelled in the ISM. Small fractions of heavy elements (iron and beyond) get produced during the explosion, and also enrich the ISM. These events are called core collapse supernovae and the most well known types are Type II, Ib and Ic. Often Type Ib and Ic are not modelled, and all SN with $M \gtrsim 8M_{\odot}$ are simply modelled as Type II supernova.

The various yields of the different type of supernovae have an important impact on the chemical evolution of Galaxies. The SFH together with an IMF determines the number of stars in a given mass range at any given time, and therefore the number of Type II SN. When the SN Type II rate is combined with the theoretical yields of these explosive events, this gives a prediction of the amount of metals ejected into the ISM at each point in time. To a first approximation, tracing each of the elements will all produce a similar MDF (§2.1), but each with a different effective yield. For iron, the story is a bit more complicated since this element is also produced in Type Ia SN. Independent of the exact model of the Type Ia SN, the progenitor is an intermediate mass star ($< 8 M_{\odot}$). These stars can live up to several Gyr, which is much longer than the Type II progenitors. The Type Ia SN events therefore have a significant delay compared to the Type II SN between their birth and explosion. This clearly violates the IRA approximation, making the iron yield not well suited for simple chemical evolution models like those presented in §2.1.

The most popular model of Type Ia SN is the accreting white dwarf (WD) scenario in a binary stellar system. The primary star (the more massive) ends its life first as a white dwarf. The secondary star (the least massive) at some point enters the red giant branch (RGB) phase. At this point, mass loss by the secondary star can accrete onto the WD remnant of the primary. If the WD then exceeds the Chandrasekhar mass ($\sim 1.4 M_{\odot}$) even the electron pressure is not able to sustain the star in hydrostatic equilibrium. Fusion in the star begins again, but the rise in temperature does not affect the pressure of the degenerate matter. This leads to a thermal runaway process which eventually causes the star to form large amounts of iron (and small amounts of other elements) which are ejected at high velocities into the ISM. Understanding the contribution of this process to the chemical evolution of galaxies depends on the number of binary stars in a system, the mass distribution of primary and secondary stars as well as the exact mechanism of mass transport.

In the next section, we will briefly present the theoretical yields used in this

²Multiples of ${}^4\text{He}$ cores: O, Ne, Mg, Si, S, Ar, Ca and Ti. Although usually they are limited to those which can be easily measured: O, Mg, Si, Ca and Ti.

report.

2.2.1 Intermediate mass yields

van den Hoek and Groenewegen (1997) calculated the theoretical yields for stars of masses $0.8 - 8M_{\odot}$ and metallicities $Z = 0.001 - 0.04$. The various dredge-up phases bring metals (and helium) to the surface where they get ejected into the IGM at their PN phase and due to stellar winds. Yields are calculated for H, ^4He , ^{12}C , ^{13}C , ^{14}N and ^{16}O for these masses and metallicities. Their definition of a yield (p_j) is somewhat different:

$$mp_j(m, Z_j(0)) = \int_0^{\tau(m)} m_{\text{eject}}(m)Z_j(t)dt - m_{\text{eject}}(m)Z_j(0), \quad (2.13)$$

where m is mass of the star, and $\tau(m)$ its lifetime.

2.2.2 Type II supernova yields

The core-collapse supernova (CCSN) are usually only modelled as Type II SN. For our models we use the Woosley and Weaver (1995) (WW95) result, consisting of theoretical yields for element between H and Zn for a mass grid between $M = 11 - 40 M_{\odot}$ and for metallicities between $Z = 0$ and $Z = Z_{\odot}$. For stars in the range $M = 8 - 11 M_{\odot}$ we rescale the yield for the lowest mass SN model ($M = 11 M_{\odot}$ for $Z = Z_{\odot}$) by mass.

2.2.3 Type Ia supernova yields

For the Type Ia SN, we use the W7 model from Iwamoto et al. (1999) which is the updated yields from the Nomoto et al. (1984). The Ca yields for the old model for instance allowed a minimum $[\text{Ca}/\text{Fe}] \sim -0.1$, while these updated yields allow $[\text{Ca}/\text{Fe}] \sim -0.5$ like seen in Fornax (Battaglia, 2007).

2.3 Press Schechter

Cosmological N-body simulations of our Universe can be used to trace the dark matter halos in 3D. Such a simulation can be used to trace the distribution of the halos as a function of redshift (z) and mass. Press and Schechter (1974) found a simple analytical model which very accurately describes the same halo distribution. The so called 'Press Schechter Formalism' is much simpler to handle than the 3D simulations, and much faster to calculate. The Press Schechter formalism

has a small issue regarding a factor of 2, which the original authors introduced ad-hoc. Later this issue was resolved by the extended Press Schechter formalism (also called the Excursion formalism), by explaining it as a cloud in cloud issue (Bond et al., 1991). Sheth and Tormen (2002) allowed for a non-spherical collapse model, providing an even better fit to the cosmological simulations. However, to understand the idea of the Press Schechter formalism, the original version with the ad-hoc factor of two will suffice. The formalism will be used in chapter 4 to trace the number of DM halos, and relate them to the number density of galaxies of different masses for each redshift. In what follows we briefly outline the Press-Schechter formalism.

In the context of cosmological structure formation, density fields are usually expressed as the density contrast:

$$\delta(\vec{x}) = \frac{\rho(\vec{x}) - \bar{\rho}}{\bar{\rho}}, \quad (2.14)$$

where $\bar{\rho}$ is the average density. If we are interested in structure formation, we are especially interested in regions where the density perturbations exceed the critical cosmological overdensity δ_c . Assuming that the density fluctuation field is a random Gaussian field, then one can ask what the probability is that we have a density contrast larger than the critical value δ_c , i.e. what is $p(\delta > \delta_c)$? From probability theory we know this is the cumulative distribution (F) of the Gaussian probability density function (f):

$$p(\delta > \delta_c) = \int_{\delta_c}^{\infty} f(\delta, \sigma_\delta) d\delta = F(\delta_c) \quad (2.15)$$

where σ_δ is the standard deviation of δ at a redshift of $z = 0$. For a Gaussian distribution, substituting $\nu = \frac{\delta}{D(z)\sigma_\delta}$, where $D(z)$ is the density growth factor³, gives F at every redshift:

$$F(\delta_c, z) = \int_{\nu_c}^{\infty} \frac{1}{\sqrt{2\pi}} e^{-\frac{1}{2}\nu^2} d\nu = \frac{1}{2} \text{Erfc}\left(\frac{\nu_c}{\sqrt{2}}\right), \quad (2.16)$$

where Erfc is the complementary error function and the variance is:

$$\sigma_\delta^2 = \xi(|x| = 0) = \int_0^{\infty} \frac{d^3k}{(2\pi)^3} P(k), \quad (2.17)$$

and ξ is the two-point correlation function, and $P(k)$ the power spectrum. This variance is not very meaningful for our use, and may even diverge for standard

³Some authors choose to include the $D(z)$ dependence in δ_c or σ_δ .

models (of course this can never be the case in reality). It is more meaningful to speak of the variance on a certain scale or mass.

Now we need to rephrase our previous question as follows: What is the probability that we find a perturbation of at least δ_c when we filter the density field on a mass scale M_f (i.e. look at masses above a certain filter mass M_f)?

$$p(\delta > \delta_c, M_f, z) = \int_{\delta_c}^{\infty} f(\delta, \sigma_{\delta, M}, M_f) d\delta = F(\delta_c, M_f). \quad (2.18)$$

Transforming this into a pdf, and dropping the $_f$ subscript for M_f :

$$\begin{aligned} p(M, z) dM &= \frac{\partial F(M)}{\partial M} dM = \frac{\partial v}{\partial M} \frac{1}{\sqrt{2\pi}} e^{-\frac{1}{2}v^2} dM \\ &= \frac{v}{\sigma} \frac{\partial \sigma}{\partial M} \frac{1}{\sqrt{2\pi}} e^{-\frac{1}{2}v^2} dM \end{aligned} \quad (2.19)$$

Converting this fraction to a comoving number density:

$$\begin{aligned} n(M, z) dM &= 2 \frac{\bar{\rho}}{M} p(M, z) dM \\ &= 2 \frac{\bar{\rho}}{M^2} v \frac{M}{\sigma} \frac{\partial \sigma}{\partial M} \frac{1}{\sqrt{2\pi}} e^{-\frac{1}{2}v^2} dM, \\ &= 2 \frac{\bar{\rho}}{M^2} v \frac{\partial \ln \sigma}{\partial \ln M} \frac{1}{\sqrt{2\pi}} e^{-\frac{1}{2}v^2} dM, \end{aligned} \quad (2.20)$$

where $\bar{\rho}$ is the average comoving density, and the factor two is needed for normalisation (see Bond et al. (1991) for the Excursion formalism which does not need an ad-hoc factor of two).

Sheth and Tormen (2002) allowed for a non-spherical collapse, and fitted the following analytical formula to their simulations:

$$n_{\text{ST}} = 2 \frac{1}{\sqrt{\pi}} \frac{\bar{\rho}}{M^2} \sqrt{v'/2} \frac{\partial \ln \sigma}{\partial \ln M} A (1 + (v')^{-p}) e^{-\frac{1}{2}v'} \quad (2.21)$$

where $v' = av^2$, and $p = 0.3$, $a = 0.707$ and $A = 0.322$.

The redshift dependence is hidden in v , via the linear density growth factor $D(z)$, which can be calculated from:

$$D(z) \propto H(z) \int_z^{\infty} \frac{1+z'}{H^3(z')} dz', \quad (2.22)$$

where $D(z=0) = 1$ and $H(z)$ is the Hubble parameter:

$$H^2(z) = H_0^2 (\Omega_{\text{m},0}(1+z)^3 + \Omega_{\Lambda,0}), \quad (2.23)$$

where $\Omega_{m,0}$ and $\Omega_{\Lambda,0}$ are the matter and Dark Energy densities, with values taken from Spergel et al. (2007).

The transfer function $T(k)$ is used to describe how to transform a primordial power spectrum to a later power spectrum incorporating structure growth:

$$P(k) = T(k)^2 P_{\text{primordial}}(k), \quad (2.24)$$

for which we use the BBKS (Bardeen et al., 1986) fitting formula:

$$T(k) = \frac{\ln(1 + 2.34q)}{2.34q(1 + 3.89q + (16.1q)^2 + (5.46q)^3 + (6.71q)^4)^{1/4}}, \quad (2.25)$$

where q is defined as $q = k/\Gamma$, and Γ can be approximated by:

$$\Gamma = \Omega_{m,0}h, \quad (2.26)$$

and h is related to the Hubble constant ($H_0 = 100 \cdot h$ km/s/Mpc). For the primordial power spectrum we use $P_{\text{primordial}}(k) \propto k$.

If we express variance in Fourier space and $\hat{W}(k)$ as our filter function, we get:

$$\sigma_{\delta}^2(M) = \int_0^{\infty} \frac{k^2 dk}{2\pi^2} P_{\text{primordial}}(k) T(k)^2 |\hat{W}|^2(k), \quad (2.27)$$

where we will use a tophat filter throughout this report.

All we need to do now is to normalise the power spectrum. We need to know the variance for at least one scale. The commonly used value is σ_8 , which is the standard deviation when the universe is filtered on a scale of $R = 8h^{-1}$ Mpc. Note that all length scales and masses are expressed in terms of h^{-1} and therefore k is in units of h Mpc $^{-1}$. We use $\sigma_8 = 0.761$ from Spergel et al. (2007) to normalise the power spectrum, and therefore the variance.

A useful function is:

$$\begin{aligned} f(\delta > \delta_c, M, z) &= p(> \delta_c, M, z)M = n(\delta > \delta_c, M, z) \frac{M^2}{\bar{\rho}}, \\ &= 2 \frac{\partial \ln \sigma}{\partial \ln M} \frac{1}{\sqrt{2\pi}} v e^{-\frac{1}{2}v^2} dM \end{aligned} \quad (2.28)$$

which is called the multiplicity function, which can be interpreted as the mass fraction of collapsed halos in the Universe per unit (natural) logarithmic bin, since $pdM = pM d \ln M$. In Fig. 2.4 we show the multiplicity function for three redshifts for the Standard Press-Schechter formalism, and for Sheth Tormen2002 for 3 different redshifts. At redshift $z = 0$, most of the mass is in $10^{14}h^{-1} M_{\odot}$ objects, i.e. clusters, while at $z = 10$ most of it is in $10^8h^{-1} M_{\odot}$ objects, which is of the order of a dwarf galaxy like Sculptor. If we look at the (comoving) number density in Fig. 2.5, we see that the high mass object are outnumbered at all redshifts. Object of $10^{8-10} M_{\odot}$ are thus important at redshift $z = 10 - 6.5$, around the epoch of reionization (EoR).

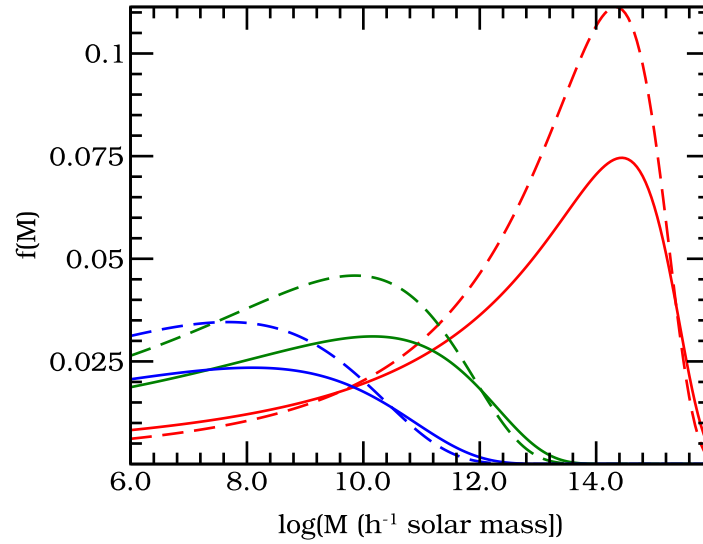


Figure 2.4: Multiplicity function. Standard Press-Schechter formalism (dashed line) and Sheth and Tormen (solid) for three redshifts: $z = 0$ (red), $z = 6$ (green), $z = 15$ (blue).

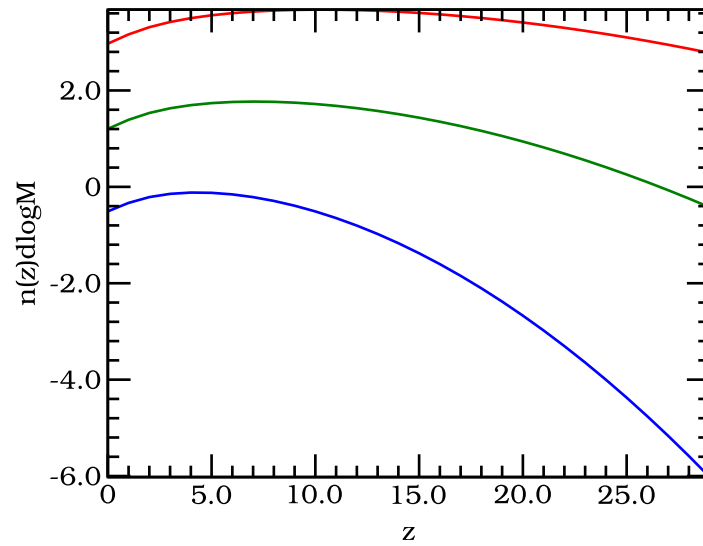


Figure 2.5: Number density per Mpc^3 per logarithmic mass bin for: $10^6 h^{-1} M_{\odot}$ (red), $10^8 h^{-1} M_{\odot}$ and $10^{10} h^{-1} M_{\odot}$.

Chapter 3

Sculptor

In this section we will explore the chemical evolution of the Sculptor dwarf spheroidal (dSph) galaxy. Sculptor was first discovered by Shapley (1938) together with Fornax, also a dSph. dwarf spheroidal galaxies have no current star formation, very low HI content, low luminosities, and are believed to contain large amounts of Dark Matter. Like many of the other dSphs, Sculptor is very close to the Milky Way, at a distance of 79 kpc (Mateo, 1998). This makes Sculptor and other dSph galaxies excellent objects to study since, due to their proximity and diffuse structure, their stellar population can be easily resolved. Sculptor also has the advantage of being at high (southern) galactic latitude (see Fig. 3.1), such that extinction and foreground contamination is expected to be low. This made it possible for the Dwarf galaxy Abundances and Radial-velocities Team (DART) to obtain photometric and spectroscopic data for Sculptor for large numbers of stars (Tolstoy et al. (2004), Battaglia (2007), Hill et al., in preparation). Previous spectroscopic studies had collected spectra for only a few stars (Armandroff and Costa, 1986; Aaronson and Olszewski, 1987; Quéloz et al., 1995; Tolstoy et al., 2001; Shetrone et al., 2003; Tolstoy et al., 2003). DART now has 91 high resolution spectra, and 470 low resolution spectra for RGB stars in Sculptor, covering a much larger fraction of the galaxy area than previous studies.

Galactic chemical evolution (GCE) models of Sculptor have mainly been based upon parameters, chosen such that abundance patterns could be matched (Lanfranchi and Matteucci, 2004; Fenner et al., 2006). The small numbers of stars available to these authors however did not allow tight constraints on the the models. We combine this new larger sample of stars having available spectroscopy, with an empirical star formation history (SFH) to create a more constrained GCE model. Using this model we can make a prediction of the amount gas inflow for Sculptor.

In §3.1 we will discuss how we used the available photometric and spectroscopic abundance data. Galactic contamination is cleaned up in the photometry

using a simple isochrone fitting routine. High resolution (HR) and low resolution (LR) iron abundances measured over different parts of the galaxy are compared to see how the two measurements can affect the total iron content and its distribution. We combine the photometry and metallicities to create a more representative sample of the whole galaxy, which is needed because of the metallicity gradient in Sculptor. Using an existing relative SFH with photometry and stellar models, we calculate the absolute SFH in §3.2. Combing the SFH with theoretical yields (§2.2) we create GCE models that can be compared to Sculptor. We chose to implement the GCE model using a simulation instead of purely analytically. The modest number of stars in Sculptor ($\sim 10^6$) make it possible to store individual stars in computer memory. This model has the advantage of being relatively easy to create and allows us to study stochastic properties originating from the initial mass function (IMF).

3.1 Data

3.1.1 Photometry

The photometric data for Sculptor were obtained using the ESO/2.2m WFI at La Silla, between September 2003 and September 2004. See Battaglia (2007) for more details about the data reduction. Observations were made through the V and I filters covering a wide region of the galaxy out to nominal tidal radius (see the bottom panel of Fig. 3.2).

The photometric centre, the ellipticity and position angle are taken from Mateo (1998). To be able to calculate distances, we first go to the tangent plane centered on the centre of Sculptor. The so called standard coordinates (Smart, 1960, §160) in the tangent plane are defined as:

$$\xi = \frac{\cot(\delta) \sin(\alpha - \alpha_0)}{\sin(\delta_0) + \cos(\delta_0) \cot(\delta) \cos(\alpha - \alpha_0)}, \quad (3.1)$$

$$\eta = \frac{\cos(\delta_0) - \cot(\delta) \sin(\delta_0) \cos(\alpha - \alpha_0)}{\sin(\delta_0) + \cos(\delta_0) \cot(\delta) \cos(\alpha - \alpha_0)}, \quad (3.2)$$

where α and δ are longitude and latitude respectively and ξ and η point to the α and δ direction.

Instead of working with ellipses, we rotate the system back such that the minor axis points north, and than scale the minor axis by $1 - e = b/a$ (a and b being the semi-major and semi-minor axis respectively) such that a circle in this coordinate system is an ellipse with the proper orientation around the centre of Sculptor (roughly corresponding to the isodensity contours). The new coordinate system is

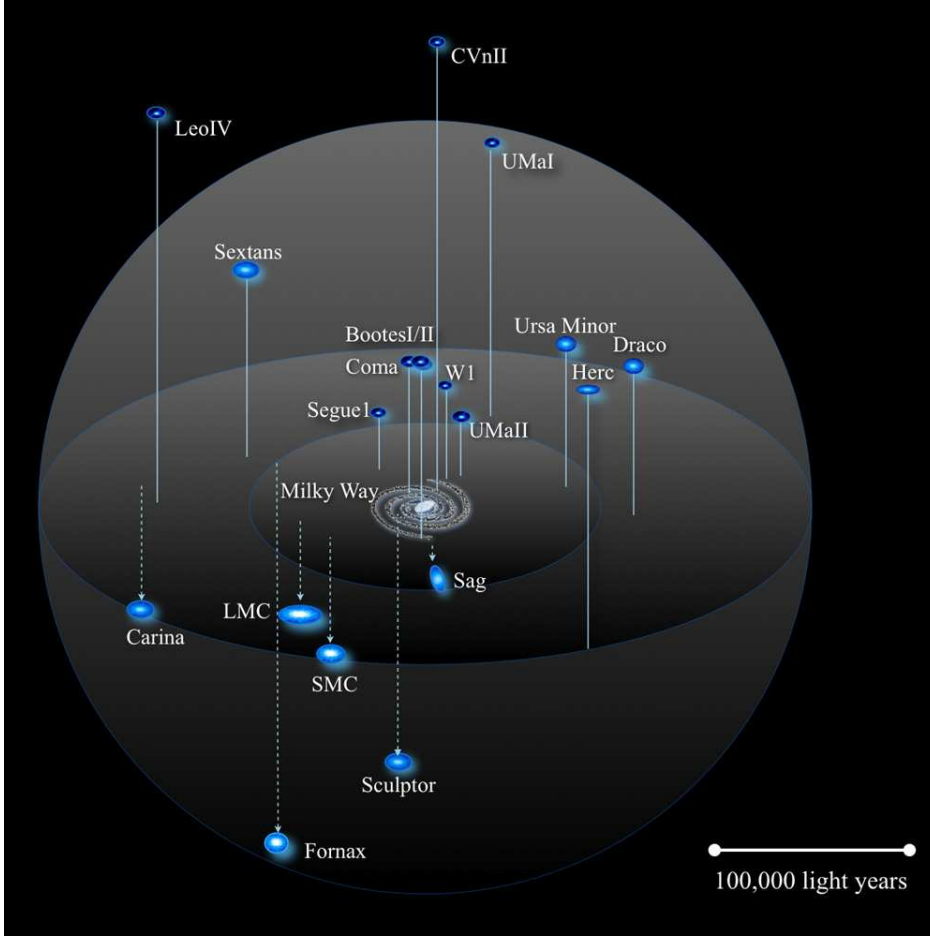


Figure 3.1: Overview of the Local Group (local neighbourhood of the Milky Way). Sculptor can be seen at high galactic latitude, and at a distance of 79kpc (100 000 lightyear \approx 30 kpc). Image from J.S. Bullock.

defined as:

$$\xi' = \xi \sin(PA - 90) - \eta \cos(PA - 90), \quad (3.3)$$

$$\eta' = (\xi \cos(PA - 90) + \eta \sin(PA - 90)) / (1 - e), \quad (3.4)$$

where PA is the position angle. Now we can define r_e (the major axis radial distance, or elliptical radius) as the distance from the centre as:

$$r_e = \sqrt{\xi'^2 + \eta'^2} \quad (3.5)$$

such that stars at constant r_e are at almost equal density regions. We can also use this coordinate system later to calculate distances between 2 stars:

$$r_e(1, 2) = \sqrt{(\xi'_1 - \xi'_2)^2 + (\eta'_1 - \eta'_2)^2} \quad (3.6)$$

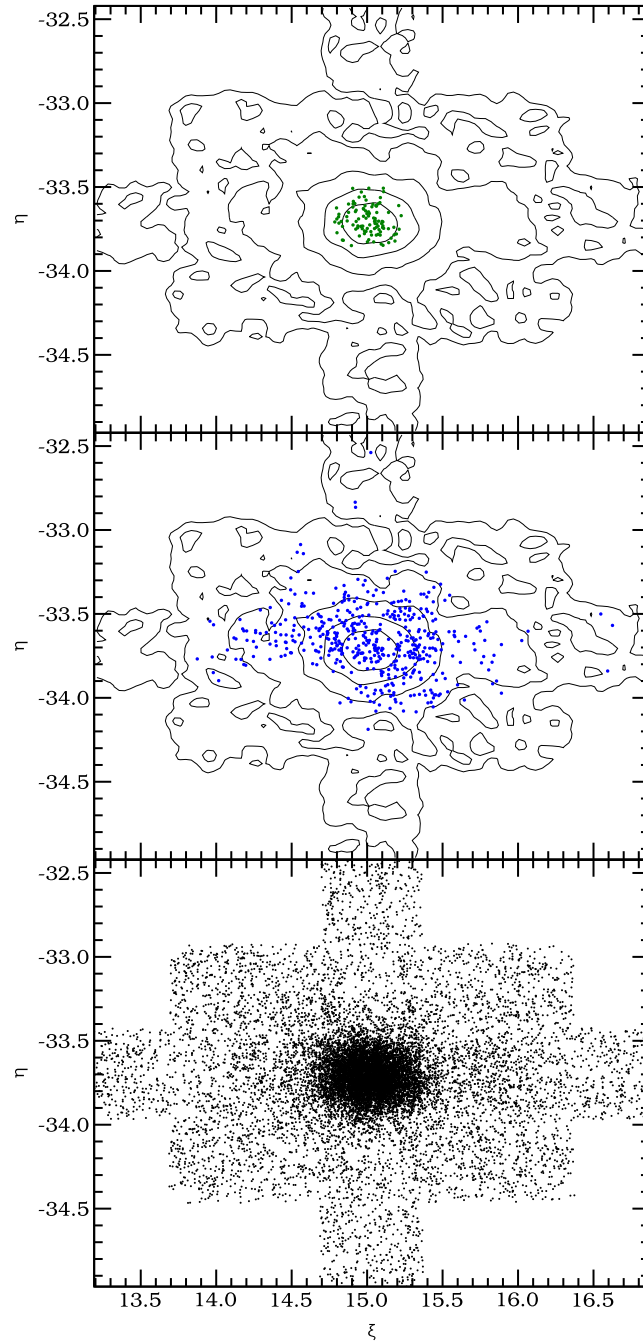


Figure 3.2: Overview of the spatial distribution of the HR spectroscopic targets (top), LR spectroscopic targets (center) and photometric data (dots in bottom panel and isocontours in the other panels) of Sculptor. Isocontour levels correspond to: 1.0%, 2.0%, 5.0%, 20.0% and 50.0%, which include 92.4%, 75.7%, 58.1%, 42.9% and 20.6% of the stars.

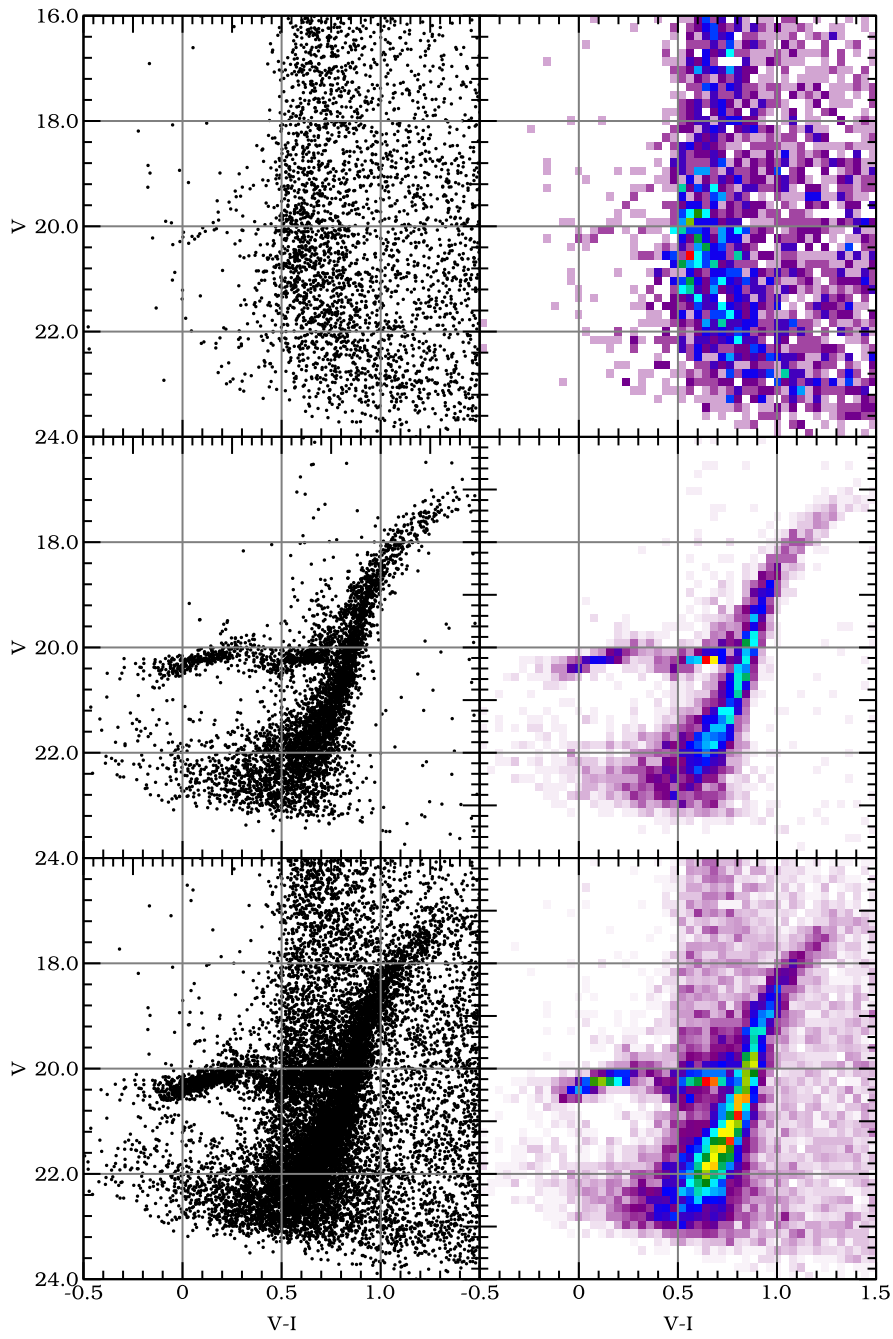


Figure 3.3: CMDs (left column) and Hess diagrams (right column) of all photometry (bottom row), the inner region ($r_e \leq 0.2^\circ$, middle row) and outer region ($> 1^\circ$, top row) of the Sculptor galaxy.

Due to the relatively close distance of Sculptor (79 kpc, Mateo (1998)), and therefore its large angular size, there is a significant foreground contamination of Milky Way stars, despite its high galactic latitude. This is illustrated in Fig. 3.3, which shows a CMD and Hess diagram for the inner part ($r_e < 0.2^\circ$) and the outer part ($r_e > 1.0^\circ$) and all of the available photometry of Sculptor. The largest fraction of the contamination lies outside the red giant branch (RGB) region as can be seen from this figure. In order to remove most of the foreground contamination, we compare them to isochrones. We use the solar scaled $Z = 0.00040$ ($[\text{Fe}/\text{H}] \approx -1.6$) Padova isochrones (Girardi et al., 2000), selecting ages in the range 6–17 Gyr. We require a minimum distance in the CMD plane, define as:

$$d_{\text{CMD}} = \sqrt{g_{V,V} (V_{\text{star}} - V_{\text{isochrone}})^2 + g_{V-I,V-I} ((V - I)_{\text{star}} - (V - I)_{\text{isochrone}})^2}, \quad (3.7)$$

where $g_{V,V}$ and $g_{V-I,V-I}$ define the metric. We choose $g_{V,V} = 15^{-2}$ and $g_{V-I,V-I} = 4.0^{-2}$, and require a minimum distance of $d_{\text{CMD}} \leq 3$. These values are chosen such that most of the galactic foreground contamination is removed. In Fig 3.4 the Hess diagram of all data (left panel) compared to the stars that match the selection criteria (right panel).

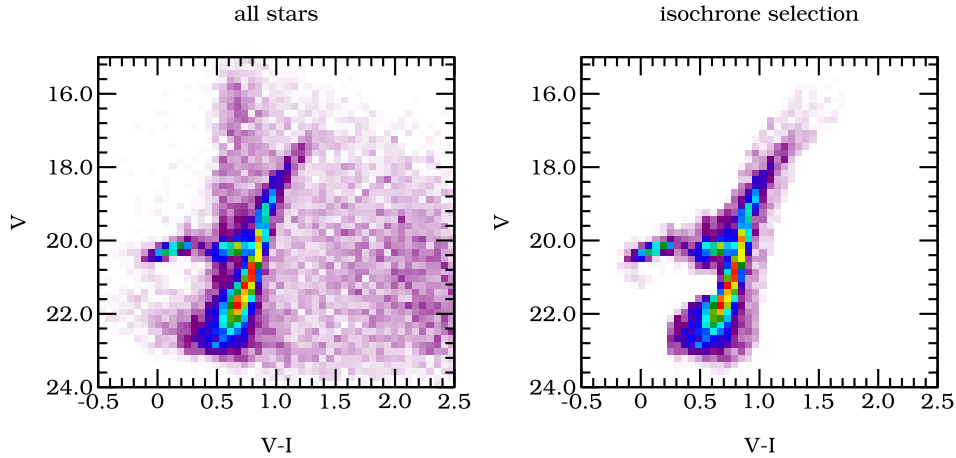


Figure 3.4: Hess diagram for Sculptor for all data (left panel) and stars withing a certain distance from the isochrones as explained in the text (right panel).

3.1.2 Metallicities

HR spectroscopic data for Sculptor were obtained using the VLT/FLAMES and VLT/UVES for DART (Tolstoy et al. (2004), Hill et al., in prep). From this data, abundances of various elements were determined. In this report we will limit

ourselves to Fe, Mg and Ca for which most of the stars have abundance measurements. Typical errors for $[\text{Fe}/\text{H}]$ and $[\text{Mg}/\text{Fe}]$ are 0.2 dex while they are 0.1 dex for $[\text{Ca}/\text{Fe}]$. These HR measurements were only obtained in the inner region of Sculptor for a total of 91 stars, as shown in the top panel of Fig. 3.2. For 470 stars, LR spectra were taken around the calcium triplet (CaT) region. Using the CaT equivalent width (EW) method (Armandroff and Costa, 1991; Rutledge et al., 1997; Battaglia et al., 2006), $[\text{Fe}/\text{H}]$ can be estimated for a much larger sample which also covers a larger region of Sculptor, as shown in the centre panel of Fig. 3.2. Uncertainties in $[\text{Fe}/\text{H}]_{\text{LR}}$ are estimated to be 0.10-0.15 dex. The LR data includes all sources that are present in the HR data set such that they can easily be compared.

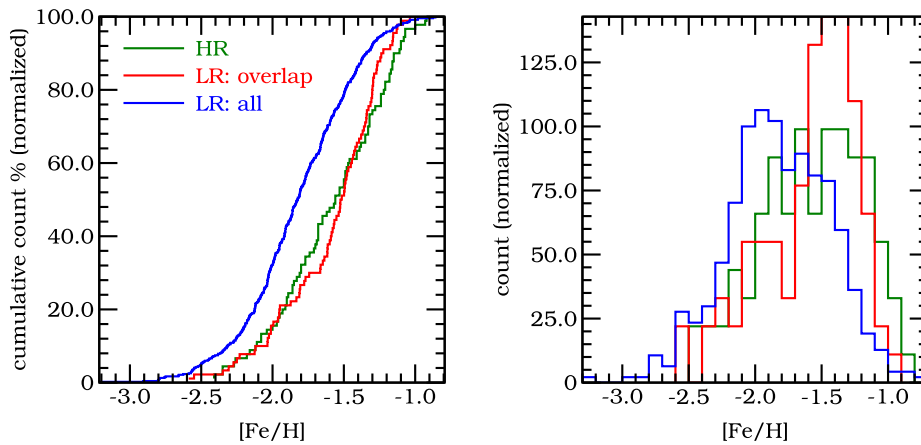


Figure 3.5: MDF for Sculptor for the LR data set (blue line) and from the overlapping data set the LR (red line) and HR data (green line). **Left:** Cumulative MDF, normalised to 100%. **Right:** Differential MDF, the area is normalised to 100%.

Given that Sculptor has a metallicity gradient (Battaglia, 2007) the question arises: What is the true metallicity ($[\text{Fe}/\text{H}]$) distribution of stars in Sculptor? And how should this be treated in a single zone GCE model. In Fig. 3.5 we show the metallicity distribution functions (MDFs) (cumulative and differential) of $[\text{Fe}/\text{H}]_{\text{HR}}$ (green line) and $[\text{Fe}/\text{H}]_{\text{LR}}$ (blue line). The HR data only cover the more metal rich inner part of Sculptor. The LR data also covers a large fraction of the outer part of Sculptor, which is low in density and therefore only a small subset of the stellar population of the whole galaxy. This means that neither sample is truly a random sample of the $[\text{Fe}/\text{H}]$ distribution of the stellar complete population Sculptor. To correct this, the density and metallicity gradient of the galaxy should be taken into account.

Figure 3.5 also shows the LR data (red line) from the overlapping set. The

HR MDF (green line) would equal the LR MDF (red line) if the CaT would agree perfectly with the HR measurements. This seems not to be the case however, as the figure shows a systematic trend: the $[\text{Fe}/\text{H}]_{\text{LR}}$ differential MDF is more peaked than the $[\text{Fe}/\text{H}]_{\text{HR}}$ distribution. From the cumulative MDF, the difference between the distribution is more clear. A two-sample Kolmogorov-Smirnov test gives a p-value of 0.38 which indicates that the deviation is not statistically significant, meaning there is a 38% chance the $[\text{Fe}/\text{H}]_{\text{LR}}$ and $[\text{Fe}/\text{H}]_{\text{HR}}$ come from the same distribution. The deviation is also not quantitatively significant for the total metal content of stars in Sculptor. The $[\text{Fe}/\text{H}]_{\text{LR}}$ gives a $\sim 10\%$ lower total iron content of the stars compared to the $[\text{Fe}/\text{H}]_{\text{HR}}$. From now on we treat the $[\text{Fe}/\text{H}]_{\text{LR}}$ and $[\text{Fe}/\text{H}]_{\text{HR}}$ as equivalent.

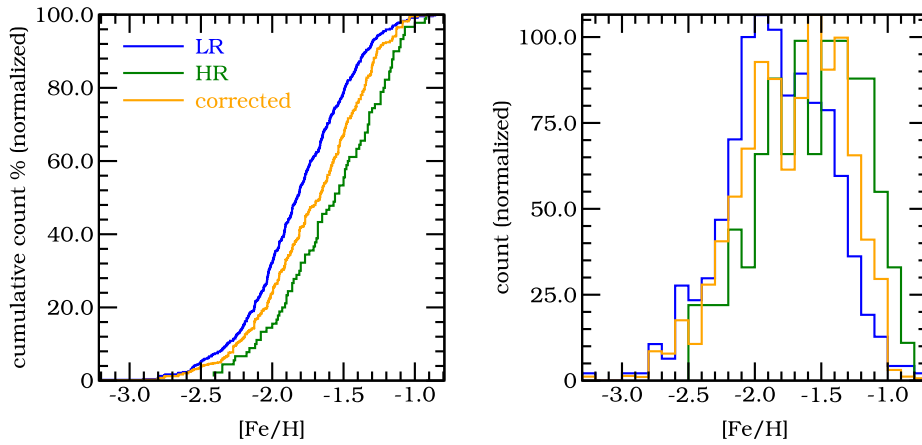


Figure 3.6: MDF for Sculptor similar to Fig. 3.5, but now including the corrected MDF as described in §3.1.2. **Left:** Cumulative MDF, normalised to 100%. **Right:** Differential MDF, the area is normalised to 100%.

Returning to the issue of having a representative sample, we implement a simple algorithm to make a correction for the MDF of Sculptor. In the ideal case, each star in the photometric data set would have its abundance measured, this is however not feasible. If the galaxy did not show any metallicity gradient, we could assign each star a random metallicity from the known distribution, and the sample would be equivalent. In the case of Sculptor, which has a metallicity gradient, the number of stars at each elliptical radius should be proportional to the density profile of the stars. To correct the MDF for the density and the metallicity gradient, we assign each star from the photometric data set a metallicity ($[\text{Fe}/\text{H}]_{\text{LR}}$) equal to the spatially nearest star from the LR data set. We required a maximum distance (in η', ξ' coordinates) of $r_e(1, 2) < 3'$. The method still leaves the stars far away from any source with known $[\text{Fe}/\text{H}]_{\text{LR}}$ without a metallicity abundance (see Fig.

3.2, centre panel). It is however a much more representative sample than using the $[\text{Fe}/\text{H}]_{\text{LR}}$ or $[\text{Fe}/\text{H}]_{\text{HR}}$ as it is observed. The MDFs (cumulative and differential) for $[\text{Fe}/\text{H}]$ are shown in Fig. 3.6. The orange line shows the corrected distribution, which lies between the $[\text{Fe}/\text{H}]_{\text{LR}}$ and $[\text{Fe}/\text{H}]_{\text{HR}}$ cumulative lines.

To do a similar correction to the $[\text{Mg}/\text{Fe}]$ and $[\text{Ca}/\text{Fe}]$ MDFs, we use the fact that $[\alpha/\text{Fe}]$ shows a correlation with $[\text{Fe}/\text{H}]$ in Sculptor (Tolstoy et al., 2006). The $[\alpha/\text{Fe}]$ abundances are assigned as follows: After the star from the photometric data set is assigned a $[\text{Fe}/\text{H}]_{\text{LR}}$ from the LR data set, we find a star in the HR data set with the closest matching $[\text{Fe}/\text{H}]_{\text{HR}}$. The $[\alpha/\text{Fe}]$ values of this HR star ($[\text{Mg}/\text{Fe}]$ and $[\text{Ca}/\text{Fe}]$) is then assigned to the star from the photometric data set. Although nothing is known about $[\alpha/\text{Fe}]$ in the outer region of Sculptor there is not reason to think it is very different from the inner region.

The corrected MDFs are shown in Fig. 3.7 as red histograms for Mg, Ca and Fe. The black line is the prediction from the Simple model using by choosing a yield that matches the corrected MDF best. This shows that Mg and Ca are very poorly described by the Simple model. Although Fe should not be accurately described by a Simple model, it seems to match the best. The low and high metallicity tails do not match however.

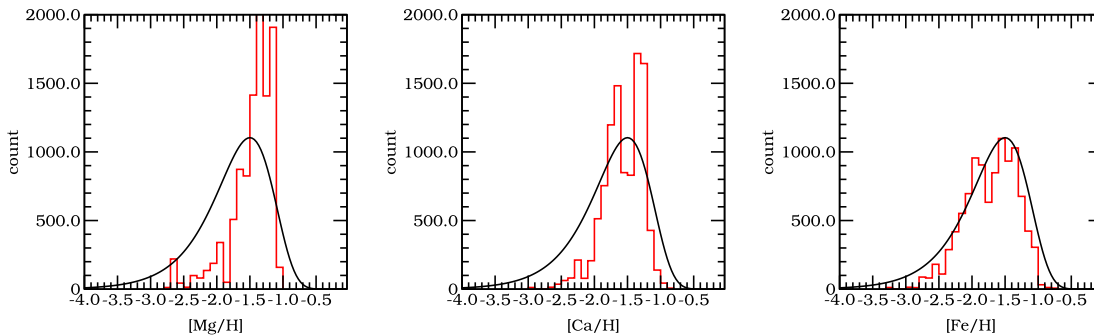


Figure 3.7: Corrected MDF for Mg, Ca and Fe as red histograms. The black line is the Simple model prediction.

3.2 The star formation history

The star formation history in the literature is given as a relative rate over time (Mateo, 1998; Tolstoy et al., 2001). These SFHs have some star formation at recent times, but these are most likely due to blue stragglers (Costa, 1984). For simplicity we will discard the SFH in the literature and use the simplified form, displayed in Fig. 3.8. We assume a single episode of a constant star formation

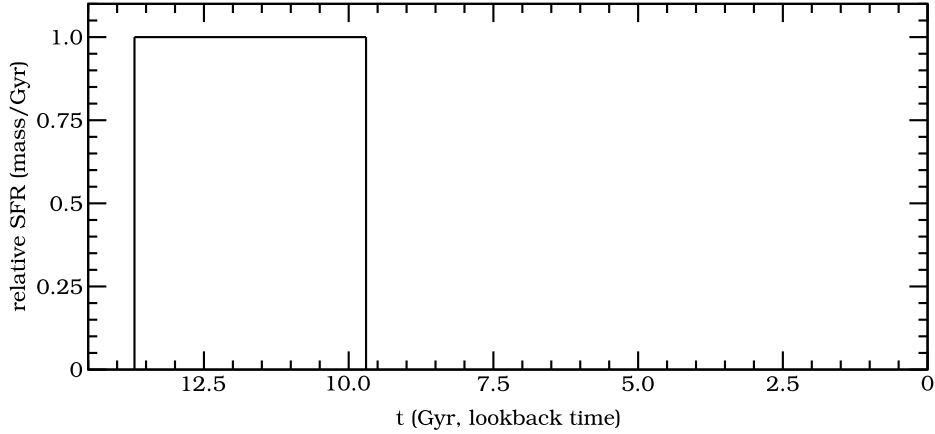


Figure 3.8: Relative SFH used for Sculptor. Star formation starts at 13.5 Gyr in our model and lasts for 4 Gyr.

rate, starting from 13.5 Gyr ago ($z \approx 15 - 20$) and lasting 4 Gyr. To be able to convert this relative SFH to a reasonable estimate of the absolute SFH we generate a synthetic CMD using the Yonsei-Yale (YY) isochrones, with $[\text{Fe}/\text{H}] = -1.6$. We fix the total number of synthetic stars to 2×10^6 , and draw the masses from an IMF. Masses drawn from the IMF are not always present in the isochrone because they have evolved away (high mass stars), or not observable (faint low mass stars). We compare the observed number of stars on the RGB with the prediction from the model. This approach is crude and may not give a very good estimate since the colour magnitude diagram (CMD) of Sculptor does not match the synthetic CMD very well, which may indicate a problem with either the photometric calibration, the isochrones or both. Assuming a Kroupa IMF (Kroupa et al., 1993) the total number of stars born in Sculptor is $N_{\text{Kroupa}} = 3\,000\,000$. Combining the flat SFH of 4 Gyr with the number of stars born, this translates to an average star formation rate (SFR) of:

$$\psi = \frac{N \int \phi(m) m dm}{4 \text{ Gyr}} = 0.00034 M_{\odot} \text{ yr}^{-1}, \quad (3.8)$$

where $\phi(m)$ is the Kroupa IMF. Although the high number of stars should give a very precise average SFR, there are uncertainties in the models and problems with the CMD and/or data as described above. This may not give a very accurate result, and the systematic uncertainty originating from this is expected to be of the order of 20% – 30%.

| Source | Mg | Ca | Fe |
|-------------------------|--------|-------|-------------------|
| theoretical WW95 yield: | 258.38 | 34.34 | 13.69 M_{\odot} |
| data: | 35.91 | 2.96 | 46.60 M_{\odot} |
| ratio: data/theoretical | 13.9% | 8.6% | 340.4% |

Table 3.1: Total metals predicted to be ejected from Type II SN in Sculptor assuming the Kroupa IMF and the SFH from §3.2 compared to total metallicities from abundance measurements and the IMF. All masses in units of M_{\odot} .

3.3 Total metallicity

Using the IMF we predict the number of Type II supernova (SN) that have occurred in Sculptor:

$$N_{\text{SNII}} = N \int_{8M_{\odot}}^{m_u} \phi(m) dm = 6970, \quad (3.9)$$

where N is the total number of stars born, and m_u is the upper mass limit of the corresponding IMF. It is interesting to know how much metals these Type II SN eject into the interstellar medium (ISM) and/or intergalactic medium (IGM). The total mass of the ejected metals for element i is (assuming a fixed metallicity or a yield that does not change with metallicity):

$$M_i = N \int_{8M_{\odot}}^{m_u} \phi(m) m_{i,\text{SNII}}(m), \quad (3.10)$$

where $m_{i,\text{SNII}}$ is the ejected mass of element i from a Type II SNe. The total metallicities using the WW95 yields for a metallicity of $Z = 0.025 Z_{\odot}$ (corresponding to $[\text{Fe}/\text{H}] = -1.6$ if $[\alpha/\text{Fe}] = 0$) can be found in the first row in Table 3.1. The second row shows the total metal content based on the abundance measurements. The third row shows the ratio between the these two in percentages. The Mg yields from WW95 are known to be low. François et al. (2004) find that these yields need to be multiplied by a factor 10. Taking this into account, and the fact that SN Type Ia produce significant amounts of Fe, it seems that a large fraction $> 90\%$ of the metals produced in Sculptor do not end up in subsequent generation of stars.

3.4 GCE model

We showed in §3.1.2 that the Simple model fails to describe all the MDFs for Sculptor. As stated in §2.1, when a metallicity distribution does not resemble the

characteristic shape of the Simple model, one or more of its assumptions have to be invalid. Changing the IMF as a function of time or any other time dependent quantity such as the metallicity of the ISM, is not a common strategy. Although common sense may suggest a dependency of the IMF on metallicity (due to cooling argument), this is not observed (Kroupa, 2001).

The Instantaneous Recycling Approximation (IRA) holds very well for metals that are mainly produced in Type II supernova explosion (SNe), such as Mg, and to good approximation also Ca. For metals that are produced in Type Ia SN or in intermediate mass stars, the approximations no longer holds. A realistic model which also includes predictions for Fe abundances, should therefore include stellar lifetimes and not assume the IRA holds. We chose to use the Padova stellar tracks (Fagotto et al., 1994a,b; Girardi et al., 1996) in our model. These stellar tracks give us the lifetime of a star as a function of initial mass and metallicity on a grid. Since the lifetime of a star is proportional to the initial mass to some power ($\tau \propto M^\alpha$), where α changes slowly with mass, interpolations for lifetimes are carried out in the $\log \tau$, $\log M$ plane.

The closed box model assumption is likely to be invalid. We have already seen in §3.3 that the total amount of metal ejected from Type II SN as predicted by the theoretical yields and the IMF is much larger than that of calculations based on spectroscopic measurements. This suggests that only $\sim 5\%$ of the metals produced by SN ejecta end up in the next generation of stars. The rest of the metals will most likely escape the galaxy, or at least the star forming regions of the galaxy. In §2.1.2 we presented two model that were able to lower the effective yield. In the leaky box model (§2.1.2.1) gas from the ISM is lost, while in the §2.1.2.2 we showed that the same can be achieved if a certain fraction of the newly produced metals directly escapes the galaxy. For the number of SN predicted in §3.3, the assumed SFH and an typical energy of a single SN of $E_{\text{SN}} = 10^{51}$ erg, the mechanical luminosity is $L_{\text{SN}} = 0.6 \times 10^{38}$ erg s^{-1} . Combining this with the results of Low and Ferrara (1999) we expect that small amounts of the ISM will be ejected, while the metal ejection will be very efficient. To model this, we let a fraction of $f_{\text{esc,Z}}$ of the metals produced by the Type II SN escape the galaxy.

A closed box model also assumes that all the gas is already present at the start of the star formation. A more realistic scenario is where only a fraction of the gas is in place due to the gravitational collapse of the gas onto the dark matter (DM) halo. Gas can then continue to accrete onto the galaxy during star formation. In §2.1.3 we showed that inflow was also able to change the characteristic shape of the MDF. Inflow of gas may thus be the crucial ingredient to reproduce the MDFs of Sculptor (see Fig. 3.7).

The cumulative MDF of Sculptor can be used to tell us what the metallicity of the ISM should be, after the formation of a given fraction of the stars. If we are above this metallicity distribution we can correct for it by letting primordial gas

flow into the galaxy (or low metallicity gas compared to the ISM). This method does require that the total amount of stars ever formed is known beforehand. This can be obtained by iteration: Make a guess, run the simulation, use the obtained star count as the input for the new simulation etc... In practise, the total number of stars ever formed does not strongly depend upon the chemical evolution history, and this number can be fixed after a single simulation run. We choose to use a MDF for a metal originating mainly from Type II SN, since the model for the progenitor of a Type Ia SN is now well known.

To model the Type Ia SN time delay model (see e.g. Matteucci and Recchi, 2001), we assume that a fraction of $f_{\text{Type Ia}}$ of stars in the mass range $M = 1.4 - 8 M_{\odot}$ explodes as a Type Ia SN. We use the W7 model from Iwamoto et al. (1999), as described in 2.2.3 for the yields.

Modifying the assumptions of the Simple model (§2.1.1) we get:

1. The system only retains a fraction $\epsilon_{Z,\text{SNII}}$ of the Type II SN and a fraction $\epsilon_{Z,\text{SNIa}}$ of the Type Ia SN ejecta. Primordial gas can flow into the system at a rate determined by reproducing the MDF of a certain metal of Sculptor.
2. Stellar lifetimes are taken into account, depending on their metallicity (Z) and their mass. A fraction of $f_{\text{Type Ia}}$ of the stars in the mass range $M = 1.4 - 8 M_{\odot}$ explode as Type Ia SN. The number of Type II SN ($M > 8 M_{\odot}$) are determined by the Kroupa IMF, where the yields are taken from (Woosley and Weaver, 1995).
3. The gas is always well mixed, meaning that any new metals are directly available for new stars (*Instantaneous Mixing Approximation (IMA)*).
4. The (Kroupa) IMF is constant in time.

Where the last two assumptions from the Simple model are maintained. The remaining free parameters are:

- (i) $\epsilon_{Z,\text{SNII}}$, the fraction of metals retained by the galaxy due to Type II SN,
- (ii) $\epsilon_{Z,\text{SNIa}}$, the fraction of metals retained by the galaxy due to Type Ia SN,
- (iii) $f_{\text{Type Ia}}$, the fraction of stars in the mass range $M = 1.4 - 8 M_{\odot}$ that explode as a Type Ia SN.

A natural choice for a simulation might be to choose a fixed time step Δt . In the case of the GCE model, this can be tricky. At each step, the time step (Δt) is multiplied by the SFR at that time ($\psi(t)$). The product of these gives you the mass of the ISM that needs to be converted to stars ($\Delta M = \psi(t) \times \Delta t$). This mass then needs to be divided over the mass samples drawn from the IMF. At some point, the

mass sample drawn from the IMF is either larger than the available mass for that time step, or leaves an amount of gas from which no star can be formed. To avoid this issue, we implement a dynamic time step. This means that we first draw a mass sample from an IMF (m_*). This mass is divided by the SFR at that time, giving us the time step ($\Delta t = m_*/\psi(t)$). In the case that no stars are formed, a minimum time step is used. A simplified version of the complete algorithm for the GCE code, including the dynamic time step, can be found in the form of pseudo code in Algorithm 1

The initial gas mass is taken as pre-enriched gas of $10^4 M_\odot$, with abundances taken from the lowest abundances found in the HR dataset. The simulation is not very sensitive to the initial mass, since the inflow can rapidly correct any discrepancies between the predicted and simulated metallicity distribution. However, a too high initial mass may lead to an incorrect metallicity distribution since the metallicity of the ISM will stay low for a longer period, predicting too many low metallicity stars.

The stochastic nature of a galaxy, induced by e.g. the IMF, may lead to different outcomes for the same initial conditions. This may cause, for instance, the Ca abundance at $[\text{Fe}/\text{H}] = -2.5$ to be different for two very similar galaxies. Our simulations are run multiple times to determine the mean inflow together with a confidence interval.

3.5 Results

As stated in §3.4, metals which are predominantly produced by Type II SN, are only influenced by inflow and $\epsilon_{\text{Z,SNII}}$ in our model. Based on the comparison between predicted and observed total metallicities (Table 3.1) we take $\epsilon_{\text{Z,SNII}} = 0.05$. The inflow is then fixed by the constraint on the cumulative metallicity distribution, for which we take the Ca element. The Mg yields are multiplied by a factor of 2.5, which is slightly higher than may be expected from Table 3.1, but seems to fit the predicted Mg distribution better. Note that the discrepancy between observed and predicted Mg yields is also found in François et al. (2004), although they find a correction factor of 7 – 10 times the WW95 yield.

The Fe distribution also depends on Type Ia SN, and is proportional to the product $\epsilon_{\text{Z,SNIa}} \times f_{\text{Type Ia}}$. This results in a degeneracy between these two parameters (increasing one by a factor of X and the other by $1/X$ gives the same yield). The degeneracy between $\epsilon_{\text{Z,SNIa}}$ and $f_{\text{Type Ia}}$ can influence the scatter in abundance patterns (especially compared to Fe, since this is mainly produced by Type Ia SN). Increasing $\epsilon_{\text{Z,SNIa}}$ and lowering $f_{\text{Type Ia}}$ such that their product stays the same, increases the scatter. The opposite will create a much smoother release of Type Ia SN ejecta (mainly Fe) in time.

Algorithm 1 Simplified pseudo code of galactic chemical evolution (GCE) model

```

1: procedure GALAXY_EVOLVE( $t_{end}, \Delta t_{min}$ )
2:    $t \leftarrow 0$ 
3:   ISM  $\leftarrow$  initial ISM
4:   shortlivedstars  $\leftarrow$  empty list
5:   while  $t < t_{end}$  do
6:      $\psi \leftarrow$  get star formation rate based on  $t$ 
7:     if  $\psi > 0$  then ▷ If we have star formation
8:        $m_* \leftarrow$  draw sample from IMF
9:        $\Delta t \leftarrow \frac{m_*}{\psi}$  ▷ Dynamic time step
10:      newstar  $\leftarrow$  create star object with mass  $m_*$ 
11:      newstar. $\tau \leftarrow$  calculate the lifetime of newstar
12:      newstar.yield  $\leftarrow$  calculate yield, based on mass and metallicity
13:      if  $t + \text{newstar}.\tau > t_{end}$  then ▷ If newstar survives until 'present
day'
14:        Store newstar information to file
15:      else
16:        Add newstar to list of shortlivedstars
17:      end if
18:    else
19:       $\Delta t \leftarrow \Delta t_{min}$  ▷ If no star formation, do a minimum timestep
20:    end if
21:    for all stars  $\in$  shortlivedstars do
22:      if star. $t_0 + \text{star}.\tau < t + \Delta t$  then ▷ If star dies in this time step
23:        ISM  $\leftarrow$  ISM + effective yield from star
24:        remove star from shortlivedstars list
25:      end if
26:    end for
27:    ISM  $\leftarrow$  ISM + infall - outflow ▷ outflow is not used for Sculptor
28:    Store ISM, infall and outflow information in files.
29:     $t \leftarrow t + \Delta t$  ▷ Update time
30:  end while
31: end procedure

```

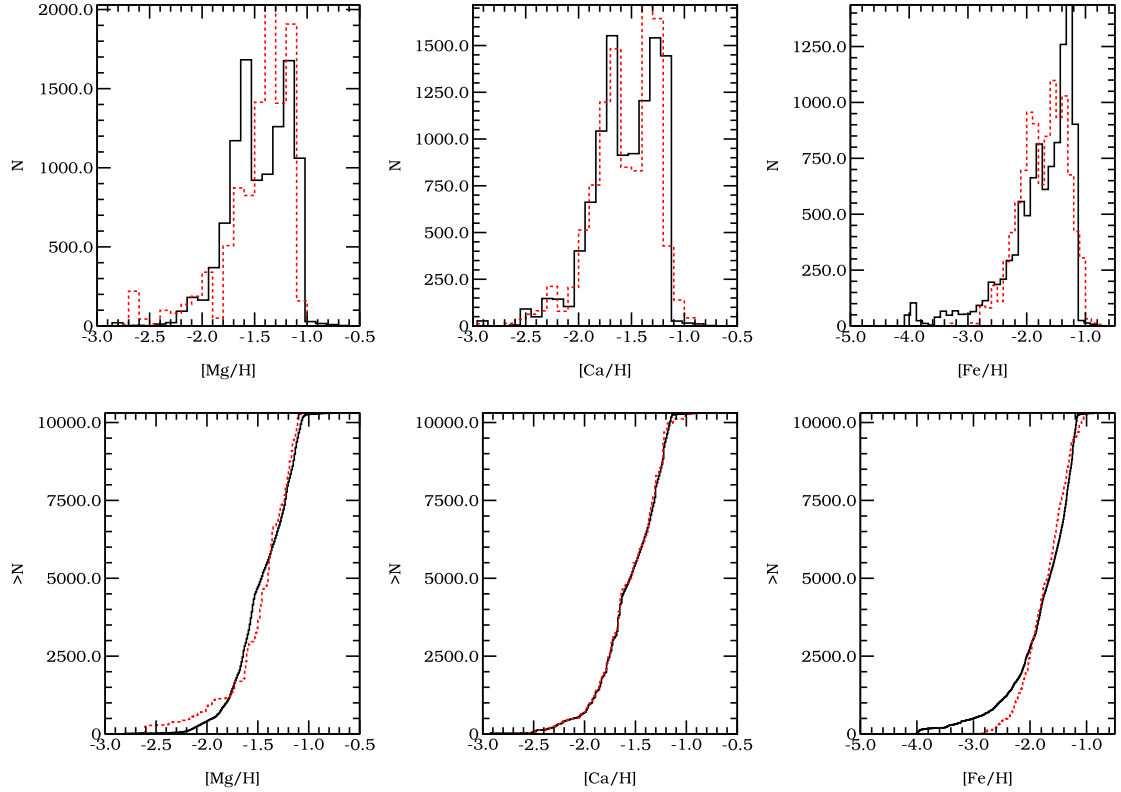


Figure 3.9: Comparison between the MDF of Sculptor (red dashed line) and Sculptor model (black solid line). **Top row:** Differential histograms of MDFs. **Bottom row:** Cumulative histograms of MDFs. From left to right, [Mg/H], [Ca/H], [Fe/H]. The [Ca/H] histogram is used as constraint and therefore reproduced. The [Mg/H] and [Fe/H] have some discrepancies, but the model trends are reasonably consistent with the data.

One may argue that because of their short lifetimes, Type II SN are likely to explode near their 'birthplace'. This may cause much of the ejecta to interact and efficiently cool with the dense gas. The Type Ia on the other hand have a larger mean lifetime, and their explosions may occur more often in less dense regions of the ISM. This may cause more of the Type Ia SN ejecta to be lost from a dwarf galaxy compared to ejecta of Type II SN. On the other hand, the simulations by Marcolini et al. (2008) suggest a different effect. First, a star burst occurs, heating the ISM. After a while, the ISM cools, and many Type Ia SN explode, forming pockets of Fe in the cold dense ISM, resulting in a high effective Fe yield. Due to the uncertainty in the Type Ia model, we simply fix $\epsilon_{Z, \text{SN Ia}} = \epsilon_{Z, \text{SN II}}$, and adjust $f_{\text{Type Ia}}$ such that the Fe distributions matches that of Sculptor.

Running the simulations we obtained the following results. In Fig. 3.9 we

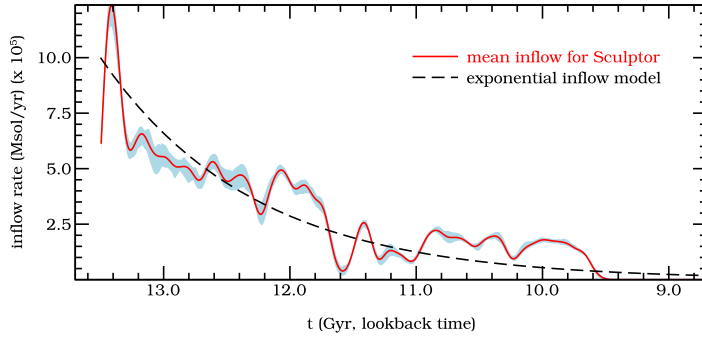


Figure 3.10: Derived inflow rate for Sculptor, using the $[\text{Ca}/\text{H}]$ MDF as a constraint. The blue region indicates the 80% confidence interval around the median originating from stochastic nature of the IMF. The red line indicates the average inflow, while the black dashed line is an exponential inflow model as described in the text.

show the MDF of Mg, Ca and Fe for Sculptor and the simulation. The distribution of Ca is well matched as expected due to our constraints. The inflow that results from this model is plotted in Fig. 3.10. The red line indicates the average inflow and the blue shading indicates the 80% confidence interval around the median. The confidence interval is based on 10 separate simulation with the same initial conditions and with different seeds for the random number generator. This creates a reflection of the stochastic nature of the IMF. The main feature of the predicted inflow is the rapid initial increase, a peak, and then a slow decline, with an almost exponential behaviour. For comparison an exponential inflow ($\dot{M}_{\text{inflow}} = \dot{M}_{\text{inflow}}(0)e^{-t/\tau}$) is also shown in the figure (dashed black line), with $\tau = 1.2$ Gyr, and $\dot{M}_{\text{inflow}}(0) = 10^{-6} \text{ M}_{\odot}/\text{yr}$. The resulting Mg and Fe yields predicted by the simulations are in reasonable agreement with the observations. However, the low metallicity tail in $[\text{Fe}/\text{H}]$ however is much too pronounced. The low metallicity tail may be caused by the fact that the Fe yield of WW95 for low Z is underestimated. This could be checked by comparing the low Z yield of WW95 to other Type II SN models. Another effect may be that the assumed SFR at early times may be too high. If the initial SFR is low then the Type Ia SNs have more time to contribute their iron yields to the ISM before many low $[\text{Fe}/\text{H}]$ stars have formed.

3.6 Discussion

The metallicity gradient in Sculptor means that the MDFs determined for spectroscopic observations are not a random sample from the galaxy. The HR data set, being centrally concentrated, is biased to the higher metallicity stars in Sculptor.

Conversely, the LR data set is biased to the lower metallicity stellar population as it covers the more extended metal poor outer regions of Sculptor. To be able to compare the MDF of a one-zone GCE model to that of Sculptor, it was necessary to make corrections to the existing measured MDFs to take into account these biases. Using a density correction we constructed a MDF that should better resemble a random sample of RGB stars in Sculptor.

Our proposed GCE model is able to reasonably reproduce the observed MDF for Mg, Ca and Fe for RGB stars in Sculptor. We use the [Ca/H] MDF to constrain the inflow and therefore the match with the data is not an outcome of the simulation but a requirement. The resulting inflow however is a prediction, and may justify the exponential form generally assumed in GCE models (e.g. Chiosi, 1980; Lanfranchi and Matteucci, 2004). Our model does depend on the exact SFH, which remains very uncertain due to its derivation from CMDs. If however the average SFH we assume does qualitatively resemble the true SFH, then the conclusion of the expected form of the inflow will most likely remain valid.

We have not discussed a possible mechanism behind the pre-enrichment of the initial gas out of which Sculptor was formed. There are two obvious scenarios that may be possible. Firstly, the pre-enrichment may be due to an older population of stars of primordial chemical composition, the so called Population III stars. In this case the enrichment would be from the galaxy itself. The pre-enrichment could also be external, from nearby galaxies that started forming stars earlier than Sculptor (see e.g. Salvadori et al., 2008). In this case the inflow should always be similar to the initial composition. This of course only affect the very low metallicity tail.

Apart from the details of the history of the chemical evolution of Sculptor, it is clear that most of the metals escape the star forming regions and probably escape the galaxy into the IGM. This makes dwarf galaxies excellent candidates for cosmic metal enrichment (Ferrara, 2008). Also the volume filling factor of metal enhanced bubbles of gas produced by dwarf galaxies is likely to be very high, making an efficient and homogeneous metal enrichment of the IGM possible. The high escape fraction of metals in Sculptor and other dwarf galaxies is reflected in the Mass-Metallicity relation (Lequeux et al., 1979). The origin of this relation, and the physics behind our $\epsilon_{Z, \text{SNII/SNIa}}$, may be the coherency of SN explosions (Ferrara et al., 2000). In smaller galaxies such as Sculptor, the spatial distance between successive SN explosions is always going to be small enough that they act coherently on the ISM allowing a large fraction of the created metals to escape. In larger galaxies such as our own, the birthplace of (Type II) SN are usually well enough separated that they rarely act coherently, such that the heated and metal enriched gas will be to cool and fall back onto the galaxy.

Chapter 4

Reionization

After just a few seconds following the Big Bang, nucleosynthesis starts forming the first elements. A few minutes later the Universe was expanded such that the low density and temperature stopped nuclear reactions. However, the high number of photons kept all atoms in an ionized state. At around $z \approx 1100$, often referred to as the last scattering surface, the CMB photons scatter on the last electrons before they recombine¹ to form a neutral Universe. From several observations we know that the hydrogen in the intergalactic medium (IGM) is highly ionized between $z = 0$ and $z \approx 6 - 7$. This period in which the Universe went from a neutral to an ionized state is called the epoch of reionization (EoR). One indicator that the Universe is ionized is the Gunn-Peterson effect (Gunn and Peterson, 1965), where neutral hydrogen leaves an imprint on the spectrum of quasar (QSO). When in the rest frame of the quasar light is emitted blue ward of the $\text{Ly}\alpha$, this light gets redshifted as it moves towards us. This causes parts of the spectrum to move to the $\text{Ly}\alpha$ line, where it can get absorbed by the neutral hydrogen. Although the neutral hydrogen fraction is low in the IGM at low redshift ($z \sim 0 - 10$), small fractions can still absorb a large fraction of the emitted light. The sudden drop of observed flux, the Gunn-Peterson trough, at $z \sim 6.3$ suggests that the Universe completed reionization at that redshift (White et al., 2003). At lower redshift the observed flux indicates that the Universe is highly ionized. A different indicator comes the the CMB. The scattering of the CMB photons on free electrons of the reionized Universe leaves an imprint on the CMB. This gives a measure for the column density of electrons between the observer and the 'start' of the EoR. Due to the projection effect it does not however give a good constrain on the precise form of the reionization history (electron density as function of z). The WMAP 3 year results (Spergel et al., 2007) give a Thompson optical depth of $\tau = 0.089 \pm 0.030$, which is for instance consistent with an instant EoR at $z \sim 11$, or a more extended

¹This is of course, the first combination between the nuclei and electrons, but it is simply a name for this process.

reionization history which ends at $z \sim 6$.

What was the source of radiation that caused the hydrogen to ionize? The most popular sources are QSOs, the metal free PopIII stars and/or PopII stars (e.g. Choudhury and Ferrara (2005, 2006) or Ciardi and Ferrara (2005) for a review). Quasars as the main source of reionization has two problems. First, the density at high redshift goes down too quickly to provide enough ionizing photons (Miralda-Escude and Ostriker, 1990). The second reason is a problem with the soft X-ray background (Dijkstra et al., 2004). If quasars would ionize the Universe at $z \approx 6$ the high energy part of their spectrum would redshift to the soft X-ray at $z = 0$, producing a background radiation higher than observed. Metal free PopIII stars are good candidates to ionize the Universe, since they have a much harder spectrum compared to the metal poor PopII stars. However, since no PopIII star is ever found, one may question its existence or the length of the epoch at which these stars formed, reducing their contribution to reionization. Other sources of ionizing radiation are possible, such as magnetic field, decaying dark matter. We will however limit this study to PopII stars, which are commonly found in galaxies and for which models exist, predicting the amount of ionizing photons they produce.

In this chapter, we will explore the role dwarf galaxies can play in the reionization of the Universe using PopII stars. The minimum requirement for reionizing the Universe is having at least a few ionizing photon per baryon, because of recombinations in the interstellar medium (ISM) and IGM. Constructing a realistic reionization model is very complicated, computational demanding and beyond the scope of the current project. Instead we focus on developing a more qualitative reionization model, leaving out processes that are neither important nor too complex.

The model we adopt is motivated by the data we discussed in chapter 3. We use the star formation rate (SFR) of Sculptor as a template for high redshift galaxies with similar dark halo masses. For the SFR for halos with different masses we use a simple scaling relation. The comoving number density of galaxies as function of mass and redshift is obtained from the Press-Schechter formalism. We then combine this with the number of ionizing photons per solar mass converted into stars using the STARBURST99 (Leitherer et al., 1999) software to construct a reionization model for the Universe. All cosmological parameters are taken from the WMAP 3 year results.

This chapter is structured as follows. In §4.1 we construct our reionization model and discuss which processes are important and which are not. The results for this model is presented in §4.2. Although we focus on a single model, we will also present results for the model using different parameters. We end with a discussion in 4.3.

4.1 Model

4.1.1 Star formation rate

The first step in our model is to have a handle on the SFR. To do so, we will use the results from chapter 3. Assuming a dark matter (DM) halo mass of Sculptor of $10^8 M_\odot$, we will use the following scaling relation for the SFR of halos of different masses.

$$\psi(M) = \psi_{\text{Scl}} \left(\frac{M}{M_{\text{Scl}}} \right)^\alpha, \quad (4.1)$$

where we take $\alpha = 1$, ψ_{Scl} and M_{Scl} are the SFR and dark halo mass of Sculptor respectively.

4.1.2 Halo mass function

Our model heavily depends on the (extended) Press-Schechter formalism for non-spherical collapse (Press and Schechter, 1974; Sheth and Tormen, 2002) (see also §2.3), giving us the comoving number density of halos as a function of halo mass and redshift. The formalism traces very well the halo distribution of cosmological DM simulations, but is much easier to work with. It is a well accepted framework within the concordance Λ CDM Universe model. The comoving number density as a function of mass and redshift from Sheth and Tormen (2002) is written as $n_{\text{ST}}(M, z)$ (see §2.3 for a details definition).

4.1.3 Ionizing photons

In order to calculate the number of ionizing photons for HII (> 13.6 eV), HeII (> 24.6 eV) and HeIII (> 54.4 eV) we use the software package STARBURST 99 (SB99) (Leitherer et al., 1999). This package uses stellar evolution models (stellar tracks) combined with stellar atmosphere models to compute spectrophotometric and related properties for stellar populations. The input for SB99 is the SFR for which we take constant value of Sculptor, and an initial mass function (IMF), for which we choose the Kroupa version, like in chapter 3. Apart from setting the isochrone to the low Z Padova isochrones ($Z = 0.0004$) all settings were kept default, as set by SB99. The ionization rate for all species is constant after a period of $\sim 10 - 20$ Myr, which is so short that we can take the ionization rate as constant in time for a given SFR. For Sculptor, this constant rate of ionizing photons is: $\log(\dot{N}_{\gamma, \text{HII}} \text{ s}^{-1}) = 49.503$, $\log(\dot{N}_{\gamma, \text{HeII}} \text{ s}^{-1}) = 48.854$ and $\log(\dot{N}_{\gamma, \text{HeIII}} \text{ s}^{-1}) = 45.178$. Translating this to number of ionizing photons per nucleon converted to stars, we get $\epsilon_{\text{SFR}, \gamma} = (1921.5, 558.0, 0.1)$ for HII, HeII and HeIII respectively (see Eq. 4.2),

or ionizing photons per solar mass converted to stars of $(228.358, 66.316, 0.014) \times 10^{58} M_{\odot}^{-1}$.

Since the ionization rate scales with the SFR, the ionization rate (per species) also scales with mass as Eq. 4.1:

$$\dot{N}_{\gamma,i}(M) = \epsilon_{\text{SFR},\gamma,i} \psi(M) = \epsilon_{\text{SFR},\gamma,i} \psi_{\text{Scl}} \left(\frac{M}{M_{\text{Scl}}} \right)^{\alpha}, \quad (4.2)$$

where again $\alpha = 1$ and $\epsilon_{\text{SFR},\gamma,i}$ is taken from the SB99 results.

The comoving ionizing photons density per unit redshift and mass becomes:

$$\frac{d^2 n_{\gamma,i,0}}{dz dM} = \dot{N}_{\gamma,i}(M) \frac{dt}{dz} n_{\text{ST}}(M, z), \quad (4.3)$$

where $\frac{dt}{dz}$ is needed to convert a rate in time to a rate in redshift. For the reionization of the Universe, the interesting quantity is the number of ionizing photon per number of atoms of species i :

$$x_{\gamma,i} = \frac{n_{\gamma,i,0}}{n_{i,0}} = \frac{1}{n_{i,0}} \int_{M=M_{\text{low}}}^{\infty} \int_{z=15.0}^{z=6.5} \frac{d^2 n_{\gamma,i}}{dz dM} dM dz, \quad (4.4)$$

where $n_{i,0}$ is the comoving number density for species i , here we chose $z = 15$ as the start of star formation and $z = 6.5$ as the end of the EoR. At high redshift the gas in the Universe is without any metals, making cooling a problem. The only efficient cooling mechanisms are atomic H, or molecular H_2 cooling. Halos which cool through the H_2 channel are able to form with virial temperature below 10^4 K. These so called mini halos and are probably heavily suppressed (Haiman and Bryan, 2006), and therefore not considered further. Atomic H cooling is only efficient above 10^4 K. Therefore we use for the lower mass limit halos with a virial temperatures above 10^4 K. Using the same approximation as Salvadori et al. (2008), the mass for halos above 10^4 K as a function of redshift is:

$$M_4(z) \approx 10^8 M_{\odot} \left(\frac{10}{1+z} \right)^{3/2}, \quad (4.5)$$

for which $M_4(z = 6.5) = 10^{8.2} M_{\odot}$ and $M_4(z = 15) = 10^{7.7} M_{\odot}$. For simplicity we take $M_{\text{low}} = 10^8 M_{\odot}$ at all redshifts. Note that after metal enrichment of the IGM or ISM by supernovae, halos with smaller masses (with virial temperature below 10^4 K) are able to cool and form stars, at later redshifts.

4.1.4 Recombination

A single ionizing photon per HI atom (and two per HeI atom) is not enough for complete reionization. The high density regions around galaxies where stars form,

make it easy for HII to recombine to HI. Only 40% of recombination enter the ground state (Type A recombination), emitting a photon which can ionize another HI atom (Tielens, 2005, §7.2). The rest of the recombinations (Type B) may lead to emitting multiple photons (including for instance the Lyman series). The recombination rate depends on the density of HII squared², which is highest in and around galaxies. This will lead to a smaller amount of ionizing photons escaping the galaxies than produced by their stars. The physics is usually parametrised by the escape fraction $f_{\text{esc},\gamma}$ of ionizing photons. This quantity can depend on mass of the hosting galaxy, or redshift. No real consensus is achieved in this area, and estimates vary between 10 – 80% (e.g. Wise and Cen, 2008), see also the discussion in Ciardi and Ferrara (2005). Instead of fixing the escape fraction, we will require that we have 1 ionizing photon per hydrogen atom at $z = 6.5$, thereby fixing $f_{\text{esc},\gamma}$ for a given model.

Apart from the high density regions near galaxies, recombination will also occur in the IGM. To see if recombination in the IGM is significant, we will compare the recombination timescale to the Hubble timescale. The recombination rate is:

$$\Gamma_{\text{recomb}} = n_e n_p \beta_B, \quad (4.6)$$

where n_e and n_p are the electron and proton number densities, and β_B is the Type B recombination rate which for hydrogen is $\beta_B = 2.6 \times 10^{-13} \text{ cm}^3 \text{ s}^{-1}$. Looking at hydrogen only, we take a characteristic recombination timescale:

$$t_{\text{recomb}} = \frac{1}{n_H \beta_B} = \frac{1}{n_{H,0} (1+z)^3 \beta_B}, \quad (4.7)$$

where $n_{H,0}$ is the comoving hydrogen number density.

In the left panel of Fig. 4.1 we plot the recombination timescale for the mean density of the Universe together with the Hubble timescale. The ratio of these two is plotted in the right panel of this figure. From this we see that although the recombination timescale is only smaller than the Hubble timescale at high redshifts, they are of comparable order of magnitude, and suggests recombination in the IGM will have an effect, although it will be small, as we will see in §4.2.2.

The assumption made above in the discussion about recombination in the IGM is that it is smooth. However, redistributing a smooth spatial distribution into a more clumpy configuration will increase the total recombinations, the recombination rate depends on the density squared. This is parametrised by the clumpyness factor:

$$C^2 = \frac{\langle n^2 \rangle}{\langle n \rangle^2}, \quad (4.8)$$

²Ignoring electrons contributed from other species, mainly He.

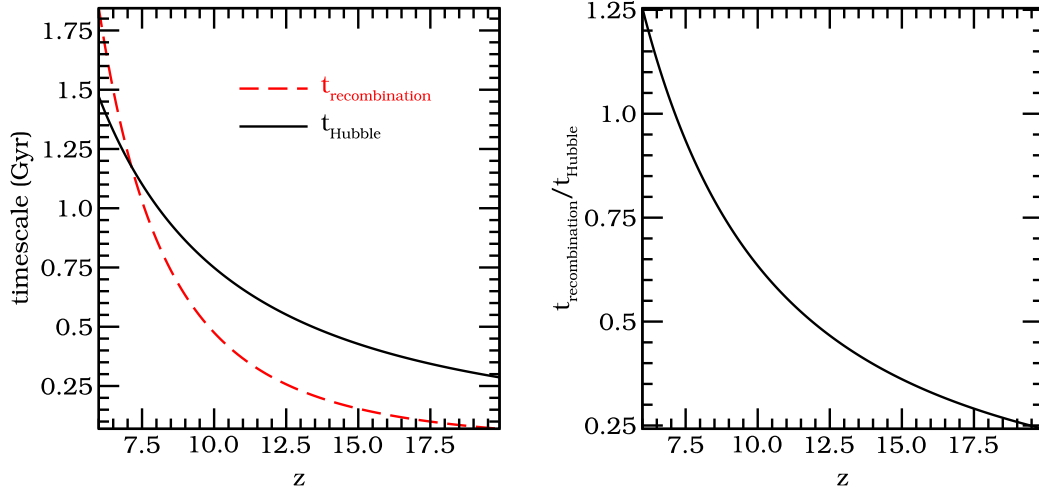


Figure 4.1: **Left:** Recombination timescale and Hubble timescale as function of redshift. **Right:** Ratio between recombination timescale and Hubble timescale. Both timescales are comparable indicating recombinations can not safely be ignored.

where the brackets indicate a spatial average. Estimates for the clumpyness factor be of the order of ~ 10 (see e.g. Haiman and Bryan, 2006), and in general depend on redshift. We will assume a smooth distribution, for which $C^2 = 1$, i.e. we assume the mean density of the Universe.

4.1.5 Mean free path

The mean free path (mfp) is defined as the average distance a photon can travel before being absorbed:

$$l_\nu = \frac{1}{n\sigma_\nu}, \quad (4.9)$$

where n is the density and σ_ν the cross section. To calculate the mfp for an ionizing photon in the IGM, we take for n the hydrogen density, and $\sigma_\nu = 6.3 \times 10^{-18} \text{ cm}^2$ the ionization cross section of hydrogen at the ionization energy (Tielens, 2005, §7.2). This gives a mfp of $l_\nu = 0.27 (1+z)^{-3} \text{ Mpc}$. On average, a photon will thus ionize in $t = l_\nu/c = 0.87 (1+z)^{-3} \text{ Myr}$, with c the speed of light, which is fast enough to be considered instantaneously.

4.1.6 Thompson optical depth

The amount of free electrons produced by the reionization between the cosmic microwave background (CMB) and the observer result in Thompson scattering,

which is expressed as the optical depth. The optical depth is defined as:

$$\tau = \int_{l_0}^{l_1} \alpha(l) dl, \quad (4.10)$$

where $\alpha(l)$ is the absorption coefficient and l the distance coordinate. For scattering of light by electrons, $\alpha(l) = n_e(l)\sigma_T$, where $n_e(l)$ is the electron density and $\sigma_T = 6.65 \times 10^{-25} \text{ cm}^2$ is the Thompson cross section. The optical depth as measured by the WMAP satellite can be compared to that predicted by a reionization model.

The proper distance elements dl is related to the comoving element $dr = a(t)dl = dl/(1+z)$. For a Friedmann-Robertson-Walker (FRW) metric the comoving distance element $dr = c a(t) dt = c dt/(1+z)$, such that $dl = c dt$. For the Thompson optical depth this gives:

$$\tau_T = \int_{z_0}^{z_1} n_e(z) \sigma_T \frac{dl}{dt} \left| \frac{dt}{dz} \right| dz, \quad (4.11)$$

$$= \int_{z_0}^{z_1} n_e(z) \sigma_T \frac{c}{H_0} \frac{1}{(1+z) \sqrt{\Omega_{m,0}(1+z)^3 + \Omega_{\Lambda,0}}} dz, \quad (4.12)$$

$$= \frac{c n_{H,0}}{H_0} \int_{z_0}^{z_1} \sigma_T x_{\text{HII}}(z) \frac{(1+z)^2}{\sqrt{\Omega_{m,0}(1+z)^3 + \Omega_{\Lambda,0}}} dz, \quad (4.13)$$

where $n_{H,0}$ is the comoving hydrogen density and $x_{\text{HII}}(z)$ the ionization fraction, defined as:

$$x_{\text{HII}}(z) = \frac{n_{\text{HII}}(z)}{n_{\text{H}}} = \frac{n_{\text{HII},0}(z)}{n_{\text{H},0}}. \quad (4.14)$$

If we want to take into account the other species (HeII and HeIII), we can extend this equation.:

$$\tau_T = \frac{c}{H_0} \int_{z_0}^{z_1} \sigma_T \{n_{\text{H},0} x_{\text{HII}}(z) + n_{\text{He},0} (x_{\text{HeII}}(z) + x_{\text{HeIII}}(z))\} \quad (4.15)$$

$$\times \frac{(1+z)^2}{\sqrt{\Omega_{m,0}(1+z)^3 + \Omega_{\Lambda,0}}} dz. \quad (4.16)$$

The time evolution of $x_{\text{HII}}(z)$, $x_{\text{HeII}}(z)$ and $x_{\text{HeIII}}(z)$ are given by our reionization model.

4.2 Results

4.2.1 Ionizing photons

We will focus on $x_{\gamma,\text{HII}}$, and see how it depends on the lower mass limits and redshift. We first define the number of ionizing photons per atom of species i ,

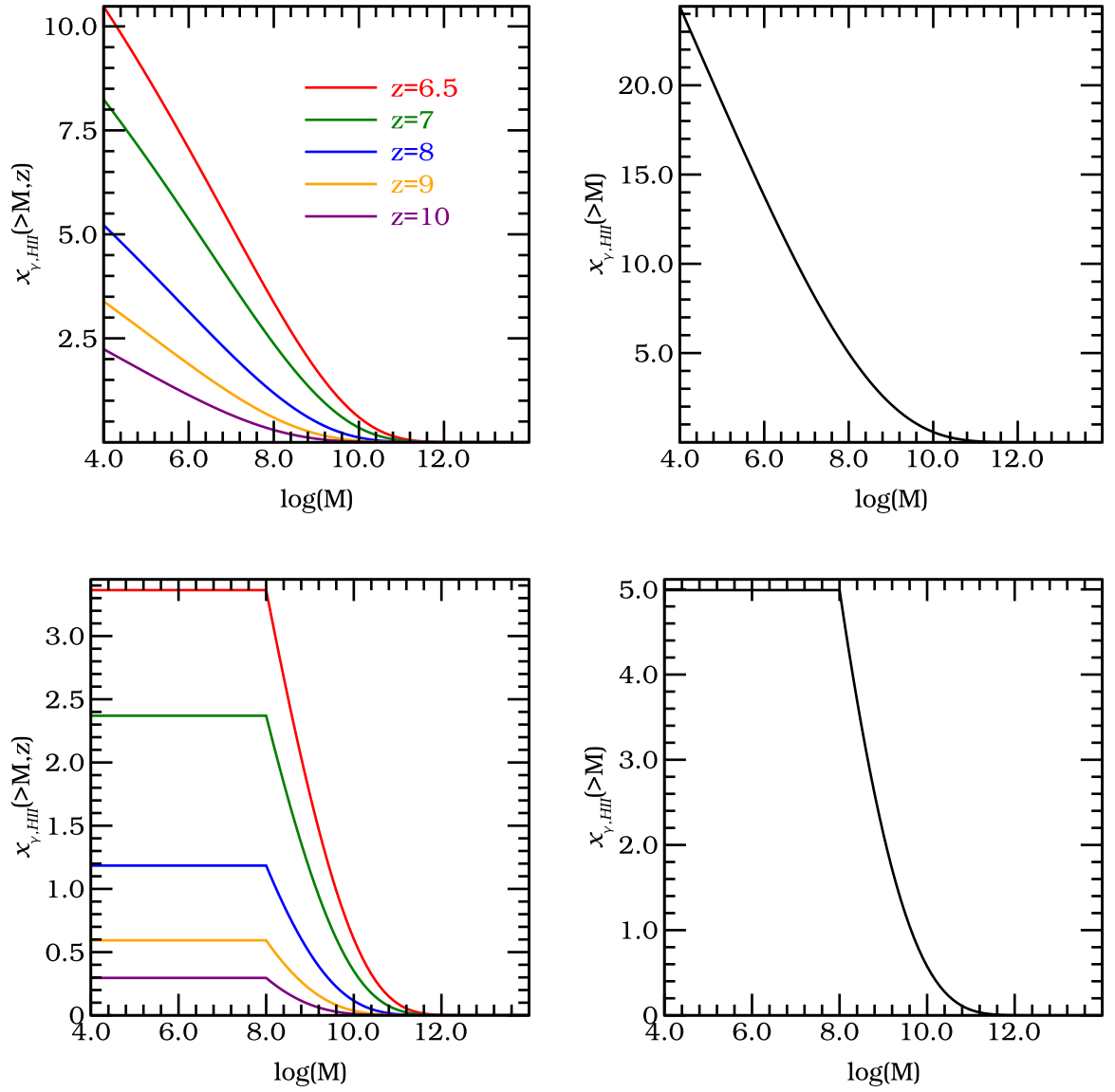


Figure 4.2: **Left column:** HII ionizing photons for all halos above a certain mass for different redshifts. **Right column:** HII ionizing photons for all halos above a certain mass in the redshift range $z = 6.5 - 15$. **Top row:** All halos. **Bottom row:** All halos above $M = 10^8 M_\odot$.

above a certain mass M , and per redshift as:

$$\begin{aligned} x_{\gamma,\text{HII}}(> M, z) &= \frac{1}{n_{\text{H},0}} \int_M^{\infty} \frac{d^2 n_{\gamma,i}}{dz dM} dM, \\ x_{\gamma,\text{HII}}(> M) &= \int_{z=15.0}^{z=6.5} x_{\gamma,i}(> M, z) dz, \end{aligned} \quad (4.17)$$

which we plot in the top panels of Fig. 4.2. In the upper left panel we see that $x_{\gamma,\text{HII}}(> M, z)$ is dominated by the lowest redshifts. Integrating over redshift, we plot $x_{\gamma,i}(> M)$ in the upper right panel. From $M = 10^{4-8} M_{\odot}$, we see that $x_{\gamma,i}$ behaves almost linear in the logarithm of the lower mass limit. The upper mass limit is taken $10^{14} M_{\odot}$, above which there is negligible contribution from ionizing photons.

A reasonable approximation for $x_{\gamma,\text{HII}}$ in the relevant redshift range is given by (see upper right plot of Fig 4.2):

$$x_{\gamma,\text{HII}} \approx 5 + (8 - \log(M_{\text{low}})) \times 5.1, \quad (4.18)$$

such that using our lower mass limit, we have 5 ionizing photons per hydrogen atom. Although we have more than 1 ionizing photons per hydrogen atom, we cannot claim this is enough to ionize the whole universe using dwarf galaxies because of the Type B recombinations.

Using the lower mass limit of $10^8 M_{\odot}$, we again calculate $x_{\gamma,i}(> M)$ and $x_{\gamma,i}(> M, z)$ in the lower panels of Fig. 4.2. From this plot it is obvious the dwarf galaxies 10^{8-10} are the main contributors to the ionizing photon production.

If we do the same analysis for HeII, we get:

$$x_{\gamma,\text{HeII}} \approx 14.9 + (8 - \log(M_{\text{low}})) \times 14.5, \quad (4.19)$$

which shows that we can easily singly ionize the HeII is we can ionize all the hydrogen. However, for HeIII we get:

$$x_{\gamma,\text{HeIII}} \approx 0.0031 + (8 - \log(M_{\text{low}})) \times 0.0031, \quad (4.20)$$

which is clearly not enough for ionize helium twice. Since there are indications that HeIII is double ionized at $z \approx 3$, we assume that it is instantaneously ionized at that redshift by a different unknown source, e.g. a quasar.

4.2.2 Recombination

In §4.1 we showed that recombination in the IGM can be relevant to the reionization history of the Universe. To quantify this, we create two simple models.

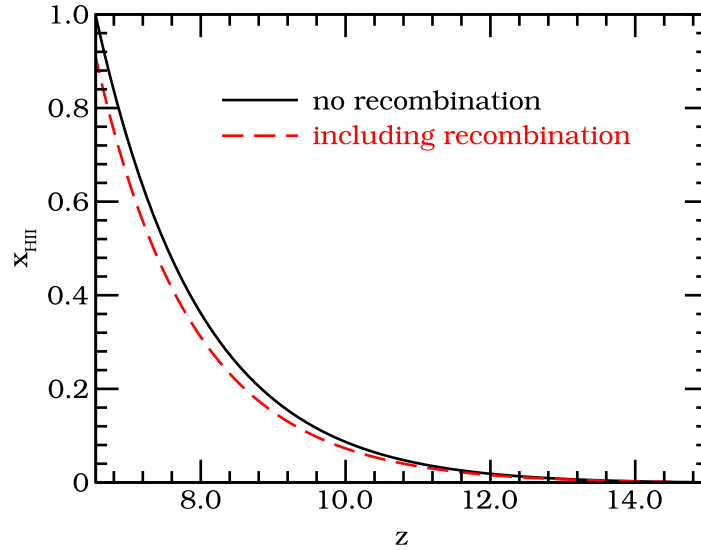


Figure 4.3: Ionization fraction of hydrogen as function of redshift without (black solid line) and with (red dashed line) recombination. With recombination, the ionization fraction of hydrogen is 90%.

The first model only takes hydrogen into account, taking the redshift and mass limits for the Press-Schechter formalism discussed above and using the SFR as given by Eq. 4.1. The second model also takes recombination of hydrogen into account. For both model we use $f_{\text{esc},\gamma} = 0.2$ such that for the model without recombination exactly 1 photon per hydrogen atom escape into the IGM, reionizing the universe at $z = 6.5$. Figure 4.3 shows the number fraction of ionized hydrogen as a function of redshift. The black solid line shows the history for the first model without recombination, while the red dashed line shows the second model taking recombination into account. The difference between the two models is that the recombination will recombine in total about $\sim 10\%$ of the ionized hydrogen. This effect is small enough that it can be neglected, since there are uncertainties in the model much larger than this, such as the $f_{\text{esc},\gamma}$.

4.2.3 Reionization model

Summarising, our reionization model is as follows:

- (i) The lower mass limit for halos is taken as $M_{\text{low}} = 10^8 M_{\odot}$, selecting only halos with virial temperatures above $T = 10^4$ K. Most of the ionizing photons come from galaxies with dark matter halos in the 10^8 – $10^{10} M_{\odot}$ range.

- (ii) Star formation starts at $z = 15$, and is proportional to the dark halo mass, normalised by the SFR of Sculptor (see Eq. 4.1).
- (iii) Recombination in the IGM is ignored, and the escape fraction ($f_{\text{esc},\gamma}$) is chosen such that at $z = 6.5$ a total number of 1 photon per baryon (H, and He) escapes the galaxies, thereby reionizing the Universe.
- (iv) Ionization are instantaneous (§4.1).
- (v) Ionization of HeIII is assumed to occur instantaneous at $z = 3$.

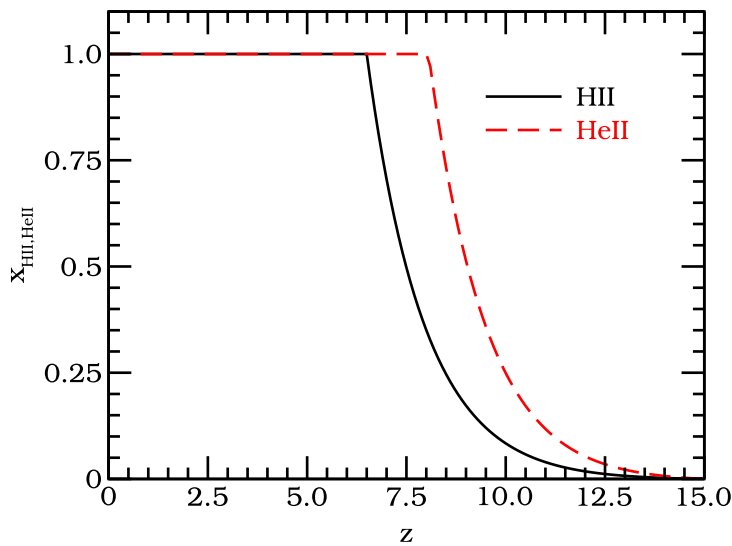


Figure 4.4: Ionization fraction as function of redshift for the final model for hydrogen (black solid line) and helium (red dashed line).

The ionization fraction for HII and HeII are plotted as function of redshift in Fig. 4.4. HeII is fully ionized at an earlier redshift of $z = 8$, while HII is fully ionized at $z = 6.5$ as imposed by the model. The HeIII is not traced at all since the number of ionizing photons to fully ionize He is far too low, about 1/5000 the amount of ionizing photons for HeII. In the left panel of Fig. 4.5 we plot the contribution to τ_T at every redshift. The black solid line shows the total contribution, while the green dashed and red dotted show the contributions from the electrons originating from H and He (HeII and HeIII) respectively. The main contribution to τ_T is found in the range $z = 2 - 8$. In the right panel, we see that the electrons before reionization already give a $\tau_T = 0.041$, which is already within 1.5σ from the WMAP 3 year results. This shows that without any reionization

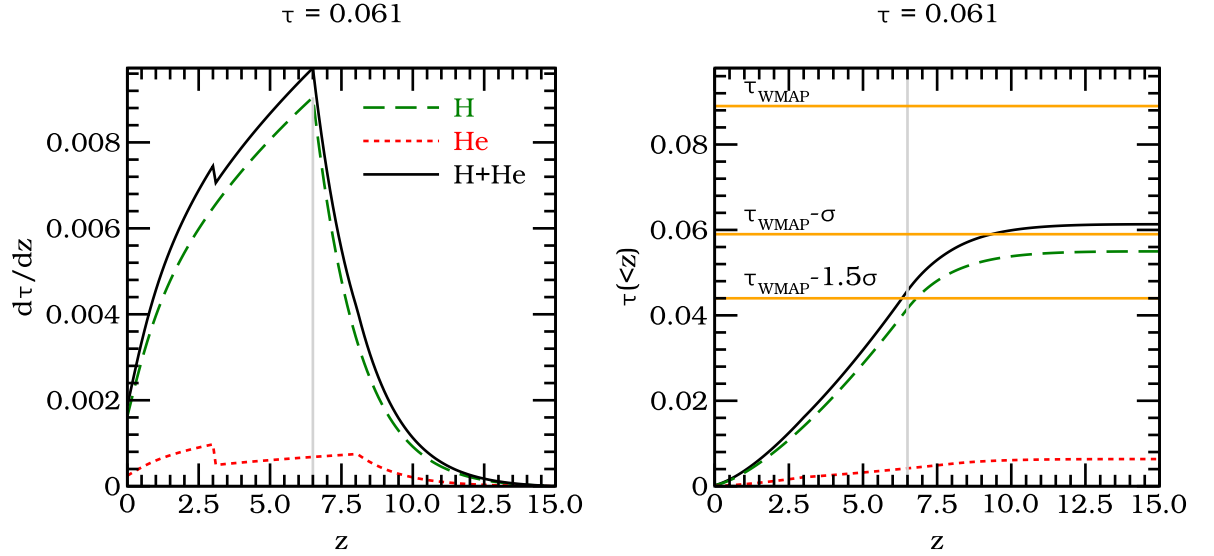


Figure 4.5: Thompson optical depth for our final model. The grey line indicates our redshift of reionization ($z = 6.5$). **Left:** Differential optical depth per redshift, showing the contribution to τ_T at each redshift. The dashed (green) line shows the contribution for HII only, and the dotted (red) line for HeII and HeIII. **Right:** Integrated optical depth, showing the contribution to τ_T below a certain redshift. The orange vertical lines indicate the WMAP 3 year value for τ_T , and the 1σ and 1.5σ below. The contribution to τ_T from electrons at $z < 6.5$ is already within 1.5σ the WMAP result.

| M_{low} | z_{start} | x_{HII} | $f_{\text{esc},\gamma}$ | τ_T |
|------------------|--------------------|------------------|-------------------------|----------|
| 10^6 | 10 | 11.46 | 0.087 | 0.059 |
| 10^6 | 15 | 13.61 | 0.073 | 0.067 |
| 10^6 | 20 | 13.79 | 0.073 | 0.068 |
| 10^8 | 10 | 4.56 | 0.219 | 0.057 |
| 10^8 | 15 | 4.98 | 0.201 | 0.061 |
| 10^8 | 20 | 4.99 | 0.200 | 0.062 |

Table 4.1: Number of ionizing photons, the escape fraction of ionizing photons and the Thompson optical depth for different models. For each model we choose a redshift at which we start forming stars (z_{start}) and a lower limit for halo masses forming stars (M_{low}).

modelling, the τ_T is already within a reasonable range. Our final optical depth for this model is $\tau_T = 0.061$, which is within 1σ of the WMAP result.

In Table 4.2.3 we listed the number of photons per hydrogen atom, the escape fraction of ionizing photons and the Thompson optical depth for different models. For each model we choose a redshift at which we start forming stars (z_{start}) and a lower limit for halo masses forming stars (M_{low}). The escape fraction is the inverse of x_{HII} such that in all cases reionization is completed at $z = 6.5$.

4.3 Discussion

Using the Press-Schechter formalism we are able to predict the number of halos as a function of mass and redshift. Each halo is assigned a SFR proportional to its mass, calibrated to the SFR of Sculptor (chapter 3). Using the Kroupa IMF and the SB99 software we calculate the amount of ionizing photons for HII, HeII and HeIII. Finding that recombination in the IGM can be neglected, the only free parameters are the lower mass limit at which halos form stars, and the escape fraction of ionizing photons. For the lower mass limit we require that the halo has a virial temperature of $T > 10^4$ K, which corresponded to a mass of $M \approx 10^8 M_{\odot}$. For this model we found that 5 ionizing photons are produced per hydrogen atom between redshift 15 and 6.5, at which we assume reionization is completed. We then choose $f_{\text{esc},\gamma}$ such that 1 ionizing photon per hydrogen atom escapes the galaxies into the IGM, thereby ionizing the Universe. The helium is singly ionized at $z = 8$, but the spectrum of the PopII stars we use is not hard enough to fully ionize it. We assume helium is fully ionized by a different source at $z = 3$. The resulting Thompson optical depth from this model, is within 1σ of the WMAP 3 year results (Spergel et al., 2007).

Using different parameters for the start of star formation and the lower mass limit for halos which form stars, we also calculate the Thompson optical depth. Although all τ_T values are within 1σ of the WMAP 3 year result, none come very close to the mean value.

We have shown that dwarf galaxies with dark halo masses in the range $M = 10^{8-10} M_{\odot}$ are able to ionize the Universe, using PopII stars. Our model may not be very realistic since we depend on many free parameters and models: The Kroupa IMF, the models used by SB99, the Press-Schechter formalism and the star formation may all have systematic errors. It is however remarkable that this very simple model predicts a few ionizing photons per hydrogen such that reionization of the Universe is possible using simply PopII stars, without tweaking many parameters. It may be that no exotic sources are needed, and that simple (low metallicity) PopII stars in dwarf galaxies are the primary source for HII and HeII reionization in the Universe.

Chapter 5

Summary

In chapter 3 we studied the chemical evolution of Sculptor. The star formation history (SFH) of Sculptor in the literature is given as a relative rate over time. To transform the relative SFH to an absolute one, we used colour magnitude diagram (CMD) analysis. The presence of a metallicity gradient in this dwarf galaxy implies that sampling from a certain region can introduce a bias in the observed metallicity distribution function (MDF). We therefore corrected the observed MDF such that we are able to compare it to a one-zone galactic chemical evolution (GCE) model. The corrected MDFs for Mg and Ca clearly does not resemble a Simple (closed box) model as described in §2.1.1. We found that a large fraction of the metals has to escape the star forming region of Sculptor in order to reproduce the total metallicity of the system. In order to reproduce the MDFs, we used an model for inflow of primordial gas as set by the Ca MDF. Our model assumes that a large fraction of the metals immediately leaves the galaxy, such that the effective yield is low. The inflow rate is characterised by large inflow rates at early time with a decreasing rate at later times. The inflow rate can be approximated by an exponential law, with a typical timescale of 1.2 Gyr.

Not only are dwarf galaxies simple system, they are also predicted to be the first galaxies to form in the concordance Λ CDM Universe. By using the Press-Schechter formalism we calculated the number of halos for a given dark halo mass and redshift. Combining this with a star formation rate (SFR) and stellar models for PopII stars to predict the rate of ionizing photons, we showed that dwarf galaxies are capable of ionizing the Universe. The results are also in reasonable agreement with the WMAP 3 year Thompson optical depth. We do not want to claim that the have found the source responsible for the epoch of reionization (EoR). Multiple sources, including as PopIII stars and/or quasars are also possible, but the high number density of $10^{8-10} M_{\odot}$ dark matter halos at high redshift makes them ideal candidates to play a large role at the EoR.

Bibliography

- M. Aaronson and E. W. Olszewski. Accurate radial velocities for carbon stars in the sculptor dwarf spheroidal. *Astronomical Journal*, 94:657–665, September 1987. URL <http://adsabs.harvard.edu/abs/1987AJ.....94..657A>.
- T. E. Armandroff and G. S. Da Costa. Metallicities for old stellar systems from ca II triplet strengths in member giants. *Astronomical Journal*, 101:1329–1337, April 1991. URL <http://adsabs.harvard.edu/abs/1991AJ....101.1329A>.
- T. E. Armandroff and G. S. Da Costa. The radial velocity, velocity dispersion, and mass-to-light ratio of the sculptor dwarf galaxy. *Astronomical Journal*, 92:777–786, October 1986. URL <http://adsabs.harvard.edu/abs/1986AJ.....92..777A>.
- J. M. Bardeen, J. R. Bond, N. Kaiser, and A. S. Szalay. The statistics of peaks of Gaussian random fields. *ApJ*, 304:15–61, May 1986. doi: 10.1086/164143.
- G. Battaglia. *Chemistry and kinematics of stars in Local Group galaxies (thesis)*. September 2007. URL <http://irs.ub.rug.nl/ppn/304002712>.
- G. Battaglia, E. Tolstoy, A. Helmi, M. J. Irwin, B. Letarte, P. Jablonka, V. Hill, K. A. Venn, M. D. Shetrone, N. Arimoto, F. Primas, A. Kaufer, P. Francois, T. Szeifert, T. Abel, and K. Sadakane. The DART imaging and CaT survey of the fornax dwarf spheroidal galaxy. *Astronomy and Astrophysics*, 459:423–440, November 2006. URL <http://adsabs.harvard.edu/abs/2006A%26A...459..423B>.
- J. R. Bond, S. Cole, G. Efstathiou, and N. Kaiser. Excursion set mass functions for hierarchical gaussian fluctuations. *Astrophysical Journal*, 379:440–460, October 1991. URL <http://adsabs.harvard.edu/abs/1991ApJ...379..440B>.
- E. Margaret Burbidge, G. R. Burbidge, William A. Fowler, and F. Hoyle. Synthesis of the elements in stars. *Reviews of Modern Physics*, 29:547–650, 1957. URL <http://adsabs.harvard.edu/abs/1957RvMP...29..547B>.
- C. Chiosi. Chemical evolution of the galactic disk - the inflow problem. *Astronomy and Astrophysics*, 83:206–216, March 1980. URL <http://adsabs.harvard.edu/abs/1980AA....83..206C>.
- T. Roy Choudhury and A. Ferrara. Experimental constraints on self-consistent reionization models. *Monthly Notices of the*

- Royal Astronomical Society*, 361:577–594, August 2005. URL <http://adsabs.harvard.edu/abs/2005MNRAS.361..577C>.
- T. Roy Choudhury and A. Ferrara. Updating reionization scenarios after recent data. *Monthly Notices of the Royal Astronomical Society*, 371:L55–L59, September 2006. URL <http://adsabs.harvard.edu/abs/2006MNRAS.371L..55C>.
- Benedetta Ciardi and Andrea Ferrara. The first cosmic structures and their effects. *Space Science Reviews*, 116:625–705, February 2005. URL <http://adsabs.harvard.edu/abs/2005SSRv..116..625C>.
- G. S. Da Costa. The age(s?) of the sculptor dwarf galaxy. *Astrophysical Journal*, 285:483–494, October 1984. URL <http://adsabs.harvard.edu/abs/1984ApJ...285..483D>.
- Mark Dijkstra, Zolton Haiman, and Abraham Loeb. A limit from the X-Ray background on the contribution of quasars to reionization. *Astrophysical Journal*, 613:646–654, October 2004. URL <http://adsabs.harvard.edu/abs/2004ApJ...613..646D>.
- F. Fagotto, A. Bressan, G. Bertelli, and C. Chiosi. Evolutionary sequences of stellar models with new radiative opacities. III. $Z=0.0004$ and $Z=0.05$. *A&AS*, 104:365–376, April 1994a.
- F. Fagotto, A. Bressan, G. Bertelli, and C. Chiosi. Evolutionary sequences of stellar models with new radiative opacities. IV. $Z=0.004$ and $Z=0.008$. *A&AS*, 105:29–38, May 1994b.
- Yeshe Fenner, Brad K. Gibson, Roberto Gallino, and Maria Lugaro. Cosmological implications of dwarf spheroidal chemical evolution. *Astrophysical Journal*, 646:184–191, July 2006. URL <http://adsabs.harvard.edu/abs/2006ApJ...646..184F>.
- Andrea Ferrara. Cosmic metal enrichment. volume 255, pages 86–99, June 2008. URL <http://adsabs.harvard.edu/abs/2008IAUS..255...86F>.
- Andrea Ferrara, Max Pettini, and Yuri Shchekinov. Mixing metals in the early universe. *Monthly Notices of the Royal Astronomical Society*, 319:539–548, December 2000. URL <http://adsabs.harvard.edu/abs/2000MNRAS.319..539F>.
- P. François, F. Matteucci, R. Cayrel, M. Spite, F. Spite, and C. Chiappini. The evolution of the Milky Way from its earliest phases: Constraints on stellar nucleosynthesis. *A&A*, 421:613–621, July 2004. doi: 10.1051/0004-6361:20034140.

- L. Girardi, A. Bressan, C. Chiosi, G. Bertelli, and E. Nasi. Evolutionary sequences of stellar models with new radiative opacities. VI. $Z=0.0001$. *A&AS*, 117:113–125, May 1996.
- L. Girardi, A. Bressan, G. Bertelli, and C. Chiosi. Evolutionary tracks and isochrones for low- and intermediate-mass stars: From 0.15 to 7 msun, and from $z=0.0004$ to 0.03. *Astronomy and Astrophysics Supplement Series*, 141:371–383, February 2000. URL <http://adsabs.harvard.edu/abs/2000A&AS..141..371G>.
- J. E. Gunn and B. A. Peterson. On the Density of Neutral Hydrogen in Intergalactic Space. *ApJ*, 142:1633–1641, November 1965. doi: 10.1086/148444.
- Zoltan Haiman and Greg L. Bryan. Was star formation suppressed in High-Redshift minihalos? *Astrophysical Journal*, 650:7–11, October 2006. URL <http://adsabs.harvard.edu/abs/2006ApJ...650....7H>.
- A. Helmi, M. J. Irwin, E. Tolstoy, G. Battaglia, V. Hill, P. Jablonka, K. Venn, M. Shetrone, B. Letarte, N. Arimoto, T. Abel, P. Francois, A. Kaufer, F. Primas, K. Sadakane, and T. Szeifert. A New View of the Dwarf Spheroidal Satellites of the Milky Way from VLT FLAMES: Where Are the Very Metal-poor Stars? *ApJ*, 651:L121–L124, November 2006a. doi: 10.1086/509784.
- A. Helmi, J. F. Navarro, B. Nordström, J. Holmberg, M. G. Abadi, and M. Steinmetz. Pieces of the puzzle: ancient substructure in the Galactic disc. *MNRAS*, 365:1309–1323, February 2006b. doi: 10.1111/j.1365-2966.2005.09818.x.
- F. Hoyle. The synthesis of the elements from hydrogen. *MNRAS*, 106:343–+, 1946.
- F. Hoyle. On Nuclear Reactions Occuring in Very Hot STARS.I. the Synthesis of Elements from Carbon to Nickel. *ApJS*, 1:121–+, September 1954.
- R. A. Ibata, G. Gilmore, and M. J. Irwin. A dwarf satellite galaxy in sagittarius. *Nature*, 370:194, July 1994. URL <http://adsabs.harvard.edu/abs/1994Natur.370..194I>.
- K. Iwamoto, F. Brachwitz, K. Nomoto, N. Kishimoto, H. Umeda, W. R. Hix, and F.-K. Thielemann. Nucleosynthesis in Chandrasekhar Mass Models for Type IA Supernovae and Constraints on Progenitor Systems and Burning-Front Propagation. *ApJS*, 125:439–462, December 1999. doi: 10.1086/313278.
- Pavel Kroupa. On the variation of the initial mass function. *Monthly Notices of the Royal Astronomical Society*, 322:231–246, April 2001. URL <http://adsabs.harvard.edu/abs/2001MNRAS.322..231K>.

- Pavel Kroupa, Christopher A. Tout, and Gerard Gilmore. The distribution of low-mass stars in the galactic disc. *Monthly Notices of the Royal Astronomical Society*, 262:545–587, June 1993. URL <http://adsabs.harvard.edu/abs/1993MNRAS.262..545K>.
- Gustavo A. Lanfranchi and Francesca Matteucci. Chemical evolution of dwarf spheroidal and blue compact galaxies. *Monthly Notices of the Royal Astronomical Society*, 345:71–85, October 2003. URL <http://adsabs.harvard.edu/abs/2003MNRAS.345...71L>.
- Gustavo A. Lanfranchi and Francesca Matteucci. The predicted metallicity distribution of stars in dwarf spheroidal galaxies. *Monthly Notices of the Royal Astronomical Society*, 351:1338–1348, July 2004. URL <http://adsabs.harvard.edu/abs/2004MNRAS.351.1338L>.
- C. Leitherer, D. Schaerer, J. D. Goldader, R. M. G. Delgado, C. Robert, D. F. Kune, D. F. de Mello, D. Devost, and T. M. Heckman. Starburst99: Synthesis Models for Galaxies with Active Star Formation. *ApJS*, 123:3–40, July 1999. doi: 10.1086/313233.
- J. Lequeux, M. Peimbert, J. F. Rayo, A. Serrano, and S. Torres-Peimbert. Chemical composition and evolution of irregular and blue compact galaxies. 80:155–166, December 1979. URL <http://adsabs.harvard.edu/abs/1979A&A....80..155L>.
- Mordecai-Mark Mac Low and Andrea Ferrara. Starburst-driven mass loss from dwarf galaxies: Efficiency and metal ejection. *Astrophysical Journal*, 513:142–155, March 1999. URL <http://adsabs.harvard.edu/abs/1999ApJ...513..142M>.
- S. R. Majewski, M. F. Skrutskie, M. D. Weinberg, and J. C. Ostheimer. A Two Micron All Sky Survey View of the Sagittarius Dwarf Galaxy. I. Morphology of the Sagittarius Core and Tidal Arms. *ApJ*, 599:1082–1115, December 2003. doi: 10.1086/379504.
- A. Marcolini, A. D’Ercole, F. Brighenti, and S. Recchi. Star formation feedback and metal enrichment by types Ia and II supernovae in dwarf spheroidal galaxies: the case of Draco. *Monthly Notices of the Royal Astronomical Society*, 371:643–658, September 2006. URL <http://adsabs.harvard.edu/abs/2006MNRAS.371..643M>.
- A. Marcolini, A. D’Ercole, G. Battaglia, and B. K. Gibson. The chemical evolution of dwarf spheroidal galaxies: dissecting the inner regions and their stel-

- lar populations. *MNRAS*, 386:2173–2180, June 2008. doi: 10.1111/j.1365-2966.2008.13175.x.
- M. L. Mateo. Dwarf Galaxies of the Local Group. *ARA&A*, 36:435–506, 1998. doi: 10.1146/annurev.astro.36.1.435.
- Francesca Matteucci and Simone Recchi. On the typical timescale for the chemical enrichment from type ia supernovae in galaxies. *Astrophysical Journal*, 558:351–358, September 2001. URL <http://adsabs.harvard.edu/abs/2001ApJ...558..351M>.
- Jordi Miralda-Escude and Jeremiah P. Ostriker. What produces the ionizing background at large redshift? *Astrophysical Journal*, 350:1–22, February 1990. URL <http://adsabs.harvard.edu/abs/1990ApJ...350....1M>.
- K. Nomoto, F.-K. Thielemann, and K. Yokoi. Accreting white dwarf models of Type I supernovae. III - Carbon deflagration supernovae. *ApJ*, 286:644–658, November 1984. doi: 10.1086/162639.
- N. Prantzos. The metallicity distribution of the halo and the satellites of the Milky Way in the hierarchical merging paradigm. *A&A*, 489:525–532, October 2008. doi: 10.1051/0004-6361:20079330.
- William H. Press and Paul Schechter. Formation of galaxies and clusters of galaxies by Self-Similar gravitational condensation. *Astrophysical Journal*, 187:425–438, February 1974. URL <http://adsabs.harvard.edu/abs/1974ApJ...187..425P>.
- D. Queloz, P. Dubath, and L. Pasquini. A kinematic study of the sculptor dwarf spheroidal galaxy. *Astronomy and Astrophysics*, 300:31, August 1995.
- G. A. Rutledge, J. E. Hesser, and P. B. Stetson. Galactic globular cluster metallicity scale from the ca II triplet II. rankings, comparisons, and puzzles. *Publications of the Astronomical Society of the Pacific*, 109:907–919, August 1997. URL <http://adsabs.harvard.edu/abs/1997PASP..109..907R>.
- Stefania Salvadori, Andrea Ferrara, and Raffaella Schneider. Life and times of dwarf spheroidal galaxies. *Monthly Notices of the Royal Astronomical Society*, 386:348–358, May 2008. URL <http://adsabs.harvard.edu/abs/2008MNRAS.386..348S>.
- Maarten Schmidt. The rate of star formation. II. the rate of formation of stars of different mass. *Astrophysical Journal*, 137:758, April 1963. URL <http://adsabs.harvard.edu/abs/1963ApJ...137..758S>.

- H. Shapley. Two stellar systems of a new kind. *Nature*, 142:715–+, 1938. doi: 10.1038/142715b0.
- R. K. Sheth and G. Tormen. An excursion set model of hierarchical clustering: ellipsoidal collapse and the moving barrier. *MNRAS*, 329:61–75, January 2002. doi: 10.1046/j.1365-8711.2002.04950.x.
- Ravi K. Sheth and Giuseppe Tormen. An excursion set model of hierarchical clustering: ellipsoidal collapse and the moving barrier. *Monthly Notices of the Royal Astronomical Society*, 329:61–75, 2002. URL <http://adsabs.harvard.edu/abs/2002MNRAS.329...61S>.
- M. D. Shetrone, P. Côté, and W. L. W. Sargent. Abundance patterns in the draco, sextans, and ursa minor dwarf spheroidal galaxies. *Astrophysical Journal*, 548:592–608, February 2001. URL <http://adsabs.harvard.edu/abs/2001ApJ...548..592S>.
- Matthew Shetrone, Kim A. Venn, Eline Tolstoy, Francesca Primas, Vanessa Hill, and Andreas Kaufer. VLT/UVES abundances in four nearby dwarf spheroidal galaxies. i. nucleosynthesis and abundance ratios. *Astronomical Journal*, 125:684–706, February 2003. URL <http://adsabs.harvard.edu/abs/2003AJ....125..684S>.
- E. D. Skillman, E. Tolstoy, A. A. Cole, A. E. Dolphin, A. Saha, J. S. Gallagher, R. C. Dohm-Palmer, and M. Mateo. Deep Hubble Space Telescope Imaging of IC 1613. II. The Star Formation History. *ApJ*, 596:253–272, October 2003. doi: 10.1086/377635.
- W.M. Smart. *Text-book on spherical astronomy*. 1960.
- D. N. Spergel, R. Bean, O. Doré, M. R. Nolta, C. L. Bennett, J. Dunkley, G. Hinshaw, N. Jarosik, E. Komatsu, L. Page, H. V. Peiris, L. Verde, M. Halpern, R. S. Hill, A. Kogut, M. Limon, S. S. Meyer, N. Odegard, G. S. Tucker, J. L. Weiland, E. Wollack, and E. L. Wright. Three-Year Wilkinson Microwave Anisotropy Probe (WMAP) Observations: Implications for Cosmology. *ApJS*, 170:377–408, June 2007. doi: 10.1086/513700.
- A. Tielens. *The Physics and Chemistry of the Interstellar Medium*. Cambridge University Press, 2005.
- B. M. Tinsley. Stellar lifetimes and abundance ratios in chemical evolution. *ApJ*, 229:1046–1056, May 1979. doi: 10.1086/157039.

- Eline Tolstoy, Michael J. Irwin, Andrew A. Cole, L. Pasquini, R. Gilmozzi, and J. S. Gallagher. Using the Ca II triplet to trace abundance variations in individual red giant branch stars in three nearby galaxies. *Monthly Notices of the Royal Astronomical Society*, 327:918–938, November 2001. URL <http://adsabs.harvard.edu/abs/2001MNRAS.327..918T>.
- Eline Tolstoy, Kim A. Venn, Matthew Shetrone, Francesca Primas, Vanessa Hill, Andreas Kaufer, and Thomas Szeifert. VLT/UVES abundances in four nearby dwarf spheroidal galaxies. II. implications for understanding galaxy evolution. *Astronomical Journal*, 125:707–726, February 2003. URL <http://adsabs.harvard.edu/abs/2003AJ....125..707T>.
- Eline Tolstoy, M. J. Irwin, A. Helmi, G. Battaglia, P. Jablonka, V. Hill, K. A. Venn, M. D. Shetrone, B. Letarte, A. A. Cole, F. Primas, P. Francois, N. Arimoto, K. Sadakane, A. Kaufer, T. Szeifert, and T. Abel. Two distinct ancient components in the Sculptor dwarf spheroidal galaxy: First results from the dwarf abundances and radial velocities team. *Astrophysical Journal*, 617:L119–L122, December 2004. URL <http://adsabs.harvard.edu/abs/2004ApJ...617L.119T>.
- Eline Tolstoy, Vanessa Hill, Mike Irwin, Amina Helmi, Guiseppina Battaglia, Bruno Letarte, Kim Venn, Pascale Jablonka, Matthew Shetrone, Nobuo Arimoto, Tom Abel, Francesca Primas, Andreas Kaufer, Thomas Szeifert, Patrick Francois, and Kozo Sadakane. The dwarf galaxy abundances and radial-velocities team (DART) large programme - a close look at nearby galaxies. *The Messenger*, 123:33, March 2006. URL <http://adsabs.harvard.edu/abs/2006Msngr.123...33T>.
- L. B. van den Hoek and M. A. T. Groenewegen. New theoretical yields of intermediate mass stars. *A&AS*, 123:305–328, June 1997.
- Kim A. Venn, Mike Irwin, Matthew D. Shetrone, Christopher A. Tout, Vanessa Hill, and Eline Tolstoy. Stellar chemical signatures and hierarchical galaxy formation. *Astronomical Journal*, 128:1177–1195, September 2004. URL <http://adsabs.harvard.edu/abs/2004AJ....128.1177V>.
- R. L. White, R. H. Becker, X. Fan, and M. A. Strauss. Probing the Ionization State of the Universe at $z > 6$. *AJ*, 126:1–14, July 2003. doi: 10.1086/375547.
- John H. Wise and Renyue Cen. Ionizing photon escape fractions from high redshift dwarf galaxies. <http://adsabs.harvard.edu/abs/2008arXiv0808.2477W>, August 2008. URL <http://adsabs.harvard.edu/abs/2008arXiv0808.2477W>.

S. E. Woosley and T. A. Weaver. The Evolution and Explosion of Massive Stars. II. Explosive Hydrodynamics and Nucleosynthesis. *ApJS*, 101:181–+, November 1995. doi: 10.1086/192237.